

2 **NmeCas9 is an intrinsically high-fidelity genome editing platform**  
3  
4  
5

6 Nadia Amrani<sup>1,\*</sup>, Xin D. Gao<sup>1,\*</sup>, Pengpeng Liu<sup>3,4</sup>, Alireza Edraki<sup>1</sup>, Aamir Mir<sup>1</sup>, Raed Ibraheim<sup>1</sup>, Ankit  
7 Gupta<sup>3,#</sup>, Kanae E. Sasaki<sup>1†</sup>, Tong Wu<sup>3</sup>, Paul D. Donohoue<sup>6</sup>, Alexander H. Settle<sup>6</sup>, Alexandra M. Lied<sup>6</sup>,  
8 Kyle McGovern<sup>6,7</sup>, Chris K. Fuller<sup>6</sup>, Peter Cameron<sup>6</sup>, Thomas G. Fazzio<sup>2,3</sup>, Lihua Julie Zhu<sup>2,3,5</sup>, Scot A.  
9 Wolfe<sup>3,4</sup>, and Erik J. Sontheimer<sup>1,2,Δ</sup>

10  
11  
12  
13 <sup>1</sup>RNA Therapeutics Institute

14 <sup>2</sup>Program in Molecular Medicine

15 <sup>3</sup>Department of Molecular, Cell and Cancer Biology

16 <sup>4</sup>Department of Biochemistry and Molecular Pharmacology

17 <sup>5</sup>Program in Bioinformatics and Integrative Biology

18  
19 University of Massachusetts Medical School

20 368 Plantation Street

21 Worcester, MA 01605

22 U.S.A.

23  
24 <sup>6</sup>Caribou Biosciences, Inc.

25 2929 7<sup>th</sup> Street, Suite 105

26 Berkeley, CA 94710

27 U.S.A.

28  
29  
30  
31 \* These authors contributed equally to this manuscript

32 # Present address: bluebird bio, Cambridge, Massachusetts, USA

33 † Present address: Molecular Pathology Unit, Massachusetts General Hospital, Charlestown,  
34 Massachusetts, USA

35 <sup>7</sup>Present address: Sangamo Therapeutics, Inc., Richmond, California, USA

36  
37 <sup>Δ</sup> Correspondence: erik.sontheimer@umassmed.edu

38  
39  
40  
41  
42  
43  
44 Running title: Intrinsically precise genome editing by NmeCas9

45  
46

47 **ABSTRACT**

48

49 **Background:** The development of CRISPR genome editing has transformed biomedical research. Most  
50 applications reported thus far rely upon the Cas9 protein from *Streptococcus pyogenes* SF370 (SpyCas9). With  
51 many RNA guides, wild-type SpyCas9 can induce significant levels of unintended mutations at near-  
52 cognate sites, necessitating substantial efforts toward the development of strategies to minimize off-target  
53 activity. Although the genome-editing potential of thousands of other Cas9 orthologs remains largely  
54 untapped, it is not known how many will require similarly extensive engineering to achieve single-site  
55 accuracy within large (e.g. mammalian) genomes. In addition to its off-targeting propensity, SpyCas9 is  
56 encoded by a relatively large (~4.2 kb) open reading frame, limiting its utility in applications that require  
57 size-restricted delivery strategies such as adeno-associated virus vectors. In contrast, some genome-editing-  
58 validated Cas9 orthologs (e.g. from *Staphylococcus aureus*, *Campylobacter jejuni*, *Geobacillus stearothermophilus* and  
59 *Neisseria meningitidis*) are considerably smaller and therefore better suited for viral delivery.

60 **Results:** Here we show that wild-type NmeCas9, when programmed with guide sequences of natural  
61 length (24 nucleotides), exhibits a nearly complete absence of unintended editing in human cells, even  
62 when targeting sites that are prone to off-target activity with wildtype SpyCas9. We also validate at least  
63 six variant protospacer adjacent motifs (PAMs), in addition to the preferred consensus PAM (5'-N<sub>4</sub>GATT-  
64 3'), for NmeCas9 genome editing in human cells.

65 **Conclusions:** Our results show that NmeCas9 is a naturally high-fidelity genome editing enzyme and  
66 suggest that additional Cas9 orthologs may prove to exhibit similarly high accuracy, even without  
67 extensive engineering.

68

69 **Keywords:** Cas9; CRISPR; sgRNA; Protospacer adjacent motif; off-target; *Neisseria meningitidis*

70

71 **BACKGROUND**

72

73       Over the past decade, clustered, regularly interspaced, short palindromic repeats (CRISPRs) have  
74    been revealed as genomic sources of small RNAs (CRISPR RNAs, crRNAs) that specify genetic  
75    interference in many bacteria and most archaea [1-3]. CRISPR sequences include “spacers,” which often  
76    match sequences of previously encountered invasive nucleic acids such as phage genomes and plasmids.  
77    In conjunction with CRISPR-associated (Cas) proteins, crRNAs recognize target nucleic acids (DNA,  
78    RNA, or both, depending on the system) by base pairing, leading to their destruction. The primary  
79    natural function of CRISPR-Cas systems is to provide adaptive immunity against phages [4, 5] and other  
80    mobile genetic elements [6]. CRISPR-Cas systems are divided into two main classes: Class 1, with large,  
81    multi-subunit effector complexes, and Class 2, with single-protein-subunit effectors [7]. Both CRISPR-  
82    Cas classes include multiple types based primarily on the identity of a signature effector protein. Within  
83    Class 2, the Type II systems are the most abundant and the best characterized. The interference function  
84    of Type II CRISPR-Cas systems requires the Cas9 protein, the crRNA, and a separate non-coding RNA  
85    known as the trans-activating crRNA (tracrRNA) [8-10]. Successful interference also requires that the  
86    DNA target (the “protospacer”) be highly complementary to the spacer portion of the crRNA, and that  
87    the PAM consensus be present at neighboring base pairs [11, 12].

88       Following the discovery that Type II interference occurs via double-strand breaks (DSBs) in the  
89    DNA target [9], the Cas9 protein was shown to be the only Cas protein required for Type II interference,  
90    to be manually reprogrammable via engineered CRISPR spacers, and to be functionally portable between  
91    species that diverged billions of years ago [10]. Biochemical analyses with purified Cas9 confirmed its role  
92    as a crRNA-guided, programmable nuclease that induces R-loop formation between the crRNA and one  
93    dsDNA strand, and that cleaves the crRNA-complementary and noncomplementary strands with its  
94    HNH and RuvC domains, respectively [13, 14]. *In vitro* cleavage reactions also showed that the tracrRNA  
95    is essential for DNA cleavage activity, and that the naturally separate crRNA and tracrRNA could retain  
96    function when fused into a single-guide RNA (sgRNA) [14]. Several independent reports then showed

97 that the established DSB-inducing activity of Cas9 could be elicited not only *in vitro* but also in living cells,  
98 both bacterial [15] and eukaryotic [16-20]. As with earlier DSB-inducing systems [21], cellular repair of  
99 Cas9-generated DSBs by either non-homologous end joining (NHEJ) or homology-directed repair (HDR)  
100 enabled live-cell targeted mutagenesis, and the CRISPR-Cas9 system has now been widely adopted as a  
101 facile genome-editing platform in a wide range of organisms [22-24]. In addition to genome editing,  
102 catalytically inactivated Cas9 (“dead” Cas9, dCas9) retains its sgRNA-guided DNA binding function,  
103 enabling fused or tethered functionalities to be delivered to precise genomic loci [25, 26]. Similar RNA-  
104 guided tools for genome manipulations have since been developed from Type V CRISPR-Cas systems  
105 that use the Cas12a (formerly Cpf1) enzyme [27].

106 Type II CRISPR-Cas systems are currently grouped into three subtypes (II-A, II-B and II-C) [7,  
107 28]. The vast majority of Cas9 characterization has been done on a single Type II-A ortholog, SpyCas9,  
108 in part due to its consistently high genome editing activity. SpyCas9’s sgRNAs typically contain a 20-nt  
109 guide sequence (the spacer-derived sequence that base pairs to the DNA target [8, 14]). The PAM  
110 requirement for SpyCas9 is 5'-NGG-3' (or, less favorably, 5'-NAG-3'), after the 3' end of the  
111 protospacer’s crRNA-noncomplementary strand [8, 14]. Based on these and other parameters, many  
112 sgRNAs directed against potentially targetable sites in a large eukaryotic genome also have near-cognate  
113 sites available to it that lead to unintended, “off-target” editing. Indeed, off-target activity by SpyCas9 has  
114 been well-documented with many sgRNA-target combinations [29, 30], prompting the development of  
115 numerous approaches to limit editing activity at unwanted sites [31-36]. Although these strategies have  
116 been shown to minimize off-targeting to various degrees, they do not always abolish it, and they can also  
117 reduce on-target activity, at least with some sgRNAs. Furthermore, each of these approaches has required  
118 extensive testing, validation, and optimization, and in some cases [33, 37, 38] depended heavily upon  
119 prior high-resolution structural characterization [39-42].

120 Thousands of other Cas9 orthologs have been documented [7, 28, 43, 44], providing tremendous  
121 untapped potential for additional genome editing capabilities beyond those offered by SpyCas9. Many  
122 Cas9 orthologs will provide distinct PAM specificities, increasing the number of targetable sites in any

123 given genome. Many pair-wise Cas9 combinations also have orthogonal guides that load into one  
124 ortholog but not the other, facilitating multiplexed applications [44-46]. Finally, some Cas9 orthologs  
125 (especially those from subtype II-C) are hundreds of amino acids smaller than the 1,368 amino acid  
126 SpyCas9 [7, 43, 44], and are therefore more amenable to combined Cas9/sgRNA delivery via a single  
127 size-restricted vector such as adeno-associated virus (AAV) [47, 48]. Finally, there may be Cas9 orthologs  
128 that exhibit additional advantages such as greater efficiency, natural hyper-accuracy, distinct activities,  
129 reduced immunogenicity, or novel means of control over editing. Deeper exploration of the Cas9  
130 population could therefore enable expanded or improved genome engineering capabilities.

131 We have used *N. meningitidis* (strain 8013) as a model system for the interference functions and  
132 mechanisms of Type II-C CRISPR-Cas systems [49-52]. In addition, we and others previously reported  
133 that the Type II-C Cas9 ortholog from *N. meningitidis* (NmeCas9) can be applied as a genome engineering  
134 platform [46, 53, 54]. At 1,082 amino acids, NmeCas9 is 286 residues smaller than SpyCas9, making it  
135 nearly as compact as SauCas9 (1,053 amino acids) and well within range of all-in-one AAV delivery. Its  
136 spacer-derived guide sequences are longer (24 nts) than those of most other Cas9 orthologs [51], and like  
137 SpyCas9, it cleaves both DNA strands between the third and fourth nucleotides of the protospacer  
138 (counting from the PAM-proximal end). NmeCas9 also has a longer PAM consensus (5'-N<sub>4</sub>GATT-3',  
139 after the 3' end of the protospacer's crRNA-noncomplementary strand) [44, 46, 51-54], leading to a lower  
140 density of targetable sites compared to SpyCas9. Considerable variation from this consensus is permitted  
141 during bacterial interference [46, 52], and a smaller number of variant PAMs can also support targeting  
142 in mammalian cells [53, 54]. Unlike SpyCas9, NmeCas9 has been found to cleave the DNA strand of  
143 RNA-DNA hybrid duplexes in a PAM-independent fashion [52, 55], and can also catalyze PAM-  
144 independent, spacer-directed cleavage of RNA [56]. Recently, natural Cas9 inhibitors (encoded by  
145 bacterial mobile elements) have been identified and validated in *N. meningitidis* and other bacteria with  
146 type II-C systems, providing for genetically encodable off-switches for NmeCas9 genome editing [57, 58].  
147 These “anti-CRISPR” (Acr) proteins [59] enable temporal, spatial, or conditional control over the  
148 NmeCas9 system. Natural inhibitors of Type II-A systems have also been discovered in *Listeria*

149 *monocytogenes* [60] and *Streptococcus thermophilus* [61], some of which are effective at inhibiting SpyCas9.

150 The longer PAM consensus, longer guide sequence, or enzymological properties of NmeCas9  
151 could result in a reduced propensity for off-targeting, and targeted deep sequencing at bioinformatically  
152 predicted near-cognate sites is consistent with this possibility [54]. A high degree of genome-wide  
153 specificity has also been noted for the dNmeCas9 platform [62]. However, the true, unbiased accuracy of  
154 NmeCas9 is not known, since empirical assessments of genome-wide off-target editing activity  
155 (independent of bioinformatics prediction) have not been reported for this ortholog. Here we define and  
156 confirm many of the parameters of NmeCas9 editing activity in mammalian cells including PAM  
157 sequence preferences, guide length limitations, and off-target profiles. Most notably, we use two empirical  
158 approaches (GUIDE-seq [63] and SITE-Seq [64] to define NmeCas9 off-target profiles and find that  
159 wild-type NmeCas9 is a high-fidelity genome editing platform in mammalian cells, with far lower levels of  
160 off-targeting than wild-type SpyCas9. These results further validate NmeCas9 as a genome engineering  
161 platform, and suggest that continued exploration of Cas9 orthologs could identify additional RNA-guided  
162 nucleases that exhibit favorable properties, even without the extensive engineering efforts that have been  
163 applied to SpyCas9 [31, 34, 35].

164

165 **RESULTS**

166

167 **Co-expressed sgRNA increases NmeCas9 accumulation in mammalian cells**

168 Previously we demonstrated that NmeCas9 (derived from *N. meningitidis* strain 8013 [51]) can  
169 efficiently edit chromosomal loci in human stem cells using either dual RNAs (crRNA + tracrRNA) or a  
170 sgRNA [53]. To further define the efficacy and requirements of NmeCas9 in mammalian cells, we first  
171 constructed an all-in-one plasmid (pEJS15) that delivers both NmeCas9 protein and a sgRNA in a single  
172 transfection vector, similar to our previous all-in-one dual-RNA plasmid (pSimple-Cas9-Tracr-crRNA;  
173 Addgene #47868) [53]. The pEJS15 plasmid expresses NmeCas9 fused to a C-terminal single-HA epitope  
174 tag and nuclear localization signal (NLS) sequences at both N- and C-termini under the control of the

175 elongation factor-1α (EF1α) promoter. The sgRNA cassette (driven by the U6 promoter) includes two  
 176 *BsmBI* restriction sites that are used to clone a spacer of interest from short, synthetic oligonucleotide  
 177 duplexes. First, we cloned three different bacterial spacers (spacers 9, 24 and 25) from the endogenous *N.*  
 178 *meningitidis* CRISPR locus (strain 8013) [51, 52] to express sgRNAs that target protospacer (ps) 9, ps24 or  
 179 ps25, respectively (Supplemental Fig. 1A). None of these protospacers have cognate targets in the human  
 180 genome. We also cloned a spacer sequence to target an endogenous genomic NmeCas9 target site (NTS)  
 181 from chromosome 10 that we called N-TS3 (Table 1). Two of the resulting all-in-one plasmids

Site	Gene or locus	Spacer Sequence of sgRNA	Target site, with PAM
NTS1B	<i>SLC9A9</i>	GGGCAUCAUGAUUUUGAACUCCU	CCTTGGCATCATGATTTGA <u>ACTCCCTATGTGATTCTA</u>
NTS1C	<i>SLC9A9</i>	GUGGUCUGGGGUACAGCCUUGGCA	TACTUGGTCTGGGTACAGCCTTGGCAT <u>CATGATT</u> TTG
NTS1C-OT1	<i>PHKG2</i>	GC <u>GGUGUGAGGUACAGCCUUGGCA</u>	TAATCGGTGTGAGGTACAGCCTTGGCAT <u>CAGGATT</u> CT
NTS3	<i>AL158836</i>	GAUGCUCAGAAAGAGGAAGCUGGU	GGGGATGCTCAGAAAGAGGAAGCTGGTTATGATTGGA
NTS4B	<i>FLJ00328</i>	GGACAGGAGUCGCCAGAGGCCGGU	GCAGGACAGGAGTCGCCAGAGGCCGGTGGATTCC
NTS4C	<i>FLJ00328</i>	GGGGCUGGUCCACGU <u>CGCCGG</u> CC	TGCGGGCTGGCTCCACGTC <u>CGCCGCCGGCGTT</u> GG
NTS5	<i>AF064860</i>	GAAACAGACUCGCAAGACUUCAGA	GACAAAACAGACTCGCAAGACTTCAGATA <u>CAGATT</u> CCA
NTS7	<i>LOC100505797</i>	GAGGGAGAGAGGUGAGCGGAUGAA	GCAAAGGGAGAGAGGTGAGCGGATGAAGGGAGATTGGT
NTS8	<i>ESPN</i>	GGACGCAAUUCCAGAGGUGAUGGG	CGGC <u>GACGCAATT</u> CCAGAGGTGATGGGAGTGA <u>TTGTC</u>
NTS9	<i>ZNHIT2</i>	GGCGCUGGUUUUUCGCAAAGCUUC	CGGC <u>CGCTGTGTT</u> TCGCAAAGCTT <u>CCGAGGATT</u> CTC
NTS10	<i>HHLA1</i>	GCAGCCAAGUUUGAGAACUGCUGU	TGTGCAGCCAAGTTGAGA <u>ACTGCTGT</u> ACAGATTCC
NTS11	<i>SMARCB1</i>	GUUCCAGUUGGGAA <u>GGGCCAGUG</u> C	TAGATTCCAGTGGGAAGGGCCAGTGCC <u>CTCCGATT</u> CCA
NTS21	<i>TNNC1</i>	GCCAGAGCUGCCGCCAGACAGUGA	CAGTCCAGAGCTGCCAGACAGTGA <u>TGCTGT</u> CTTG
NTS25	<i>AC193513</i>	GGUUUCUCAUCCUGCUUCUGCCU	CCGC <u>GTTCTCATCCTGT</u> CTGCCTAGGGATATGT
NTS26	<i>LOC105378512</i>	GUUCAAAAGUAGCGGGCGUAGGC	GTACTTCAAAGTAGCGGGCGTAGGGGGT <u>TTCTG</u>
NTS27	<i>TIE1</i>	GUUCUCCAAGCCCUCGGACCUCGU	CGGCTTCTCCAG <u>CCCTCG</u> GA <u>CTCGTGGCGT</u> CTTCT
NTS30	<i>NEK8</i>	GGGGCUCCGGAGCCCACCCCA <u>GG</u> A	CGGGGGCTCCGGAGCCCACCCCA <u>GGG</u> AGGAC <u>GGG</u> ACTTAG
NTS31	<i>POC1A</i>	GUGGAAGGUAGCUC <u>CCACCUUCC</u>	ATGGTGGGAAGTGTAGCTCCAC <u>CTTCC</u> CCAGACATAG
NTS32	<i>VEGFA</i>	GCCCCGGCUCUGGUAA <u>AGAGGG</u> A	CACACCCGG <u>CTCTGG</u> CTAA <u>AGAGGG</u> ATGGGTT <u>GG</u>
NTS33	<i>VEGFA</i>	GC <u>GGGGAGAAGGCCAGGG</u> UCACU	GGAGCGGGAGAAGGCCAGGG <u>TC</u> CCAGGATT <u>CCA</u>
NTS55	<i>CYBB</i>	GCUGGAUUACUGUGGUAGAGGG	CTAGCTGGATTACTGTGTG <u>TAGAGGGAGGT</u> GATTAGC
NTS58	<i>AAVS1</i>	GUUUGCCUGGACACCCGUUCUCC	TTTCTTGCCTGGACACCC <u>GGTCTC</u> CTGTGGATT <u>CGG</u>
NTS59	<i>AAVS1</i>	GAC <u>CCCCACAGUGGGGCCACUAGGG</u>	CTCCACCC <u>ACAGTGGG</u> CCACTAGGGACAGGATT <u>GGT</u>
STS60	<i>AAVS1</i>	GUUAAUGUGGCUCUGGUUCU	CCGGTTAATGTGG <u>CTCTGG</u> TTCT <u>GGGT</u> TAC
STS61	<i>AAVS1</i>	GU <u>CCCCUCCACCCACAGUG</u>	TCTG <u>CCCC</u> CCAC <u>ACAGTGGG</u> CCA
STS62	<i>AAVS1</i>	GGGGCCACUAGGGACAGGAU	AGTGGGG <u>CCACTAGGG</u> ACAGGATT <u>GGTGA</u>
NTS63	<i>AAVS1</i>	GAGUUAGAACUCAGGACCAACUUA	CCAAAGTTAGA <u>ACTCAGG</u> ACCAACTTATT <u>CTGATT</u> TTG
NTS64	<i>Rosa26</i>	GGCAGAU <u>CACGAGGGAAAGAGGG</u> GG	AGTTGCAGAT <u>CACGAGGGAAAGAGGG</u> AA <u>AGGGATT</u> CTC

182 **Table 1.** NmeCas9 or SpyCas9 guide and target sequences used in this study. NTS, NmeCas9 target site; STS,  
 183 SpyCas9 target site. The sgRNA spacer sequences (5'→3') are shown with their canonical lengths, and with a 5'-  
 184 terminal G residue; non-canonical lengths are described in the text and figures. Target site sequences are also 5'→3'  
 185 and correspond to the DNA strand that is non-complementary to the sgRNA, with PAM sequences underlined.  
 186  
 187 (spacer9/sgRNA and N-TS3/sgRNA), as well as a plasmid lacking the sgRNA cassette, were transiently  
 188 transfected into HEK293T cells for 48 hours, and NmeCas9 expression was assessed by anti-HA western

189 blot (Fig. 1A). As a positive control we also included a sample transfected with a SpyCas9-expressing  
190 plasmid (triple-HA epitope-tagged, and driven by the cytomegalovirus (CMV) promoter) [65] (Addgene  
191 #69220). Full-length NmeCas9 was efficiently expressed in the presence of both sgRNAs (lanes 3 and 4).  
192 However, the abundance of the protein was much lower in the absence of sgRNA (lane 2). A different  
193 Type II-C Cas9 (CdiCas9) was shown to be dramatically stabilized by its cognate sgRNA when subjected  
194 to proteolysis *in vitro* [55]; if similar resistance to proteolysis occurs with NmeCas9 upon sgRNA binding, it  
195 could explain some or all of the sgRNA-dependent increase in cellular accumulation.

196

### 197 **Efficient editing in mammalian cells by NmeCas9**

198 To establish an efficient test system for NmeCas9 activity in mammalian cells, we used a co-  
199 transfected fluorescent reporter carrying two truncated, partially overlapping GFP fragments that are  
200 separated by a cloning site [66] into which we can insert target protospacers for NmeCas9. Cleavage  
201 promotes a single-strand-annealing-based repair pathway that generates an intact GFP open reading  
202 frame (ORF), leading to fluorescence [66] that can be scored after 48 hours by flow cytometry. We  
203 generated reporters carrying three validated bacterial protospacers (ps9, ps24 and ps25, as described  
204 above) [51, 52] for transient cotransfection into HEK293T cells along with the corresponding  
205 NmeCas9/sgRNA constructs. Figure 1B shows that all three natural protospacers of NmeCas9 can be  
206 edited in human cells and the efficiency of GFP induction was comparable to that observed with SpyCas9  
207 (Fig. 1B).

208 Next, we reprogrammed NmeCas9 by replacing the bacterially-derived spacers with a series of  
209 spacers designed to target eleven human chromosomal sites with an N<sub>4</sub>GATT PAM (Table 1). These  
210 sgRNAs induced insertion/deletion (indel) mutations at all sites tested, except NTS10 (Fig. 1C, lanes 23-  
211 25), as determined by T7 Endonuclease 1 (T7E1) digestion (Fig. 1C). The editing efficiencies ranged from  
212 5% for NTS1B site to 47% in the case of NTS33 (Fig. 1D), though T7E1 tends to underestimate the true  
213 frequencies of indel formation [67]. These data confirm that NmeCas9 can induce, with variable  
214 efficiency, edits at many genomic target sites in human cells. Furthermore, we demonstrated NmeCas9

215 genome editing in multiple cell lines and via distinct delivery modes. Nucleofection of NmeCas9  
216 ribonucleoprotein (RNP) (loaded with an *in vitro*-transcribed sgRNA) led to indel formation at three sites in  
217 K562 chronic myelogenous leukemia cells and in hTERT-immortalized human foreskin fibroblasts (gift  
218 from Dr. Job Dekker) (Fig. 1E). In addition, mouse embryonic stem cells (mESCs) and HEK293T cells  
219 were transduced with a lentivirus construct expressing NmeCas9. In these cells, transient transfection of  
220 plasmids expressing a sgRNA led to genome editing (Fig. 1E). Collectively, our results show that  
221 NmeCas9 can be used for genome editing in a range of human or mouse cell lines via plasmid  
222 transfection, RNP delivery, or lentiviral transduction.

223

#### 224 **Functionality of truncated sgRNAs with NmeCas9**

225 SpyCas9 can accommodate limited variation in the length of the guide region (normally 20  
226 nucleotides) of its sgRNAs [68-71], and sgRNAs with modestly lengthened (22-nt) or shortened (17–18-nt)  
227 guide regions can even enhance editing specificity by reducing editing at off-target sites by a greater  
228 degree than they affect editing at the on-target site [68, 69]. To test the length dependence of the  
229 NmeCas9 guide sequence (normally 24 nucleotides; [51]) during mammalian editing, we constructed a  
230 series of sgRNAs containing 18, 19, 20, 21, 22, 23, and 24 nucleotides of complementarity to ps9 cloned  
231 into the split-GFP reporter plasmid (Supplemental Fig. 1B). All designed guides started with two guanine  
232 nucleotides (resulting in 1-2 positions of target non-complementarity at the very 5' end of the guide) to  
233 facilitate transcription and to test the effects of extra 5'-terminal G residues, analogous to the SpyCas9  
234 “GGN<sub>20</sub>” sgRNAs [68]. We then measured the abilities of these sgRNAs to direct NmeCas9 cleavage of  
235 the reporter in human cells. sgRNAs that have 20–23 nucleotides of target complementarity showed  
236 activities comparable to the sgRNA with the natural 24 nucleotides of complementarity, whereas sgRNAs  
237 containing 18 or 19 nucleotides of complementarity show lower activity (Fig. 2A).

238 We next used a native chromosomal target site (NTS33 in *VEGFA*, as in Figs. 1C and 1D) to test  
239 the editing efficiency of NmeCas9 spacers of varying lengths (Supplemental Fig. 1C). sgRNA constructs  
240 included one or two 5'-terminal guanine residues to enable transcription by the U6 promoter, sometimes

241 resulting in 1–2 nucleotides of target non-complementarity at the 5' end of the guide sequence. sgRNAs  
242 with 20, 21, or 22 nucleotides of target complementarity (GGN<sub>18</sub>, GGN<sub>19</sub>, and GGN<sub>20</sub>, respectively)  
243 performed comparably to the natural guide length (24 nucleotides of complementarity, GN<sub>23</sub>) at this site  
244 (Fig. 2B-C), and within this range, the addition of 1–2 unpaired G residues at the 5' end had no adverse  
245 effect. These results are consistent with the results obtained with the GFP reporter (Fig. 2A). sgRNAs with  
246 guide lengths of 19 nucleotides or shorter, along with a single mismatch in the first or second position  
247 (GGN<sub>17</sub>, GGN<sub>16</sub>, and GGN<sub>15</sub>), did not direct detectable editing, nor did a sgRNA with perfectly matched  
248 guide sequences of 17 or 14 nucleotides (GN<sub>16</sub> and GN<sub>13</sub>, respectively) (Fig. 2B-C). However, a 19-nt  
249 guide with no mismatches (GN<sub>18</sub>) successfully directed editing, albeit with slightly reduced efficiency.  
250 These results indicate that 19–26-nt guides can be tolerated by NmeCas9, but that activity can be  
251 compromised by guide truncations from the natural length of 24 nucleotides down to 17–18 nucleotides  
252 and smaller, and that single mismatches (even at or near the 5'-terminus of the guide) can be  
253 discriminated against with a 19-nt guide.

254 The target sites tested in Figs. 2A and 2B-C are both associated with a canonical N<sub>4</sub>GATT PAM,  
255 but efficient NmeCas9 editing at mammalian chromosomal sites associated with N<sub>4</sub>GCTT [53] and other  
256 variant PAMs [[54]; also see below] has also been reported. To examine length dependence at a site with  
257 a variant PAM, we varied guide sequence length at the N<sub>4</sub>GCTT-associated NTS32 site (also in *VEGFA*).  
258 In this experiment, each of the guides had two 5'-terminal G residues, accompanied by 1–2 terminal  
259 mismatches with the target sequence (Supplemental Fig. 1D). At the NTS32 site, sgRNAs with 21–24  
260 nucleotides of complementarity (GGN<sub>24</sub>, GGN<sub>23</sub>, GGN<sub>22</sub>, and GGN<sub>21</sub>) supported editing, but shorter  
261 guides (GGN<sub>20</sub>, GGN<sub>19</sub>, and GGN<sub>18</sub>) did not (Fig. 2D-E). We conclude that sgRNAs with 20 nucleotides  
262 of complementarity can direct editing at some sites (Fig. 2B-C) but not all (Fig. 2D-E). It is possible that  
263 this minor variation in length dependence can be affected by the presence of mismatched 5'-terminal G  
264 residues in the sgRNA, the adherence of the target to the canonical N<sub>4</sub>GATT PAM consensus, or both,  
265 but the consistency of any such relationship will require functional tests at much larger numbers of sites.  
266 Nonetheless, NmeCas9 guide truncations of 1–3 nucleotides appear to be functional in most cases, in

267 agreement with the results of others [54].

268

## 269 **PAM specificity of NmeCas9 in human cells**

270 During native CRISPR interference in bacterial cells, considerable variation in the N<sub>4</sub>GATT  
271 PAM consensus is tolerated: although the G1 residue (N<sub>4</sub>GATT) is strictly required, virtually all other  
272 single mutations at A2 (N<sub>4</sub>GATT), T3 (N<sub>4</sub>GATT), and T4 (N<sub>4</sub>GATT) retain at least partial function in  
273 licensing bacterial interference [46, 52]. In contrast, fewer NmeCas9 PAM variants have been validated  
274 during genome editing in mammalian cells [53, 54]. To gain more insight into NmeCas9 PAM flexibility  
275 and specificity in mammalian cells, and in the context of an otherwise identical target site and an invariant  
276 sgRNA, we employed the split-GFP readout of cleavage activity described above. We introduced single-  
277 nucleotide mutations at every position of the PAM sequence of ps9, as well as all double mutant  
278 combinations of the four most permissive single mutants, and then measured the ability of NmeCas9 to  
279 induce GFP fluorescence in transfected HEK293T cells. The results are shown in Fig. 3A. As expected,  
280 mutation of the G1 residue to any other base reduced editing to background levels, as defined by the  
281 control reporter that lacks a protospacer [(no ps), see Fig. 3A]. As for mutations at the A2, T3 and T4  
282 positions, four single mutants (N<sub>4</sub>GCTT, N<sub>4</sub>GT<sub>3</sub>T, N<sub>4</sub>GACT, and N<sub>4</sub>GATA) and two double mutants  
283 (N<sub>4</sub>GTCT and N<sub>4</sub>GACA) were edited with efficiencies approaching that observed with the N<sub>4</sub>GATT  
284 PAM. Two other single mutants (N<sub>4</sub>GAGT and N<sub>4</sub>GATG), and three double mutants (N<sub>4</sub>GCCT,  
285 N<sub>4</sub>GCTA, and N<sub>4</sub>GT<sub>3</sub>TA) gave intermediate or low efficiencies, and the remaining mutants tested were at  
286 or near background levels. We note that some of the minimally functional or non-functional PAMs (e.g.  
287 N<sub>4</sub>GAAT and N<sub>4</sub>GATC) in this mammalian assay fit the functional consensus sequences defined  
288 previously in *E. coli* [46].

289 We then used T7E1 analysis to validate genome editing at eight native chromosomal sites  
290 associated with the most active PAM variants (N<sub>4</sub>GCTT, N<sub>4</sub>GT<sub>3</sub>T, N<sub>4</sub>GACT, N<sub>4</sub>GATA, N<sub>4</sub>GTCT, and  
291 N<sub>4</sub>GACA). Our results with this set of targets indicate that all of these PAM variants tested except  
292 N<sub>4</sub>GACA support chromosomal editing (Fig. 3B and C).

293

294 **Apo NmeCas9 is not genotoxic to mammalian cells**

295 NmeCas9 and several other type II-C Cas9 orthologs have been shown to possess an RNA-  
296 dependent ssDNA cleavage (DNase H) activity *in vitro* [52, 55]. R-loops (regions where an RNA strand  
297 invades a DNA duplex to form a DNA:RNA hybrid, with the other DNA strand displaced) occur  
298 naturally during transcription and other cellular processes [72]. Since DNase H activity is independent of  
299 the tracrRNA or the PAM sequence, it is theoretically possible that it could degrade naturally-occurring  
300 R-loops in living cells. Global degradation of R-loops in cells could result in an increase in DNA damage  
301 detectable by increased  $\gamma$ H2AX staining [73]. To test whether the DNase H activity of NmeCas9 could  
302 lead to an increase in  $\gamma$ H2AX, we transduced mouse embryonic stem cells E14 (mESCs) with lentiviral  
303 plasmids expressing NmeCas9 and dNmeCas9 (which lacks DNase H activity; [52]). mESCs are ideal for  
304 this purpose as R-loops have been extensively studied in these cells and have been shown to be important  
305 for differentiation [74]. We performed  $\gamma$ H2AX staining of these two cell lines and compared them to  
306 wildtype E14 cells. As a positive control for  $\gamma$ H2AX induction, we exposed wildtype E14 cells to UV, a  
307 known stimulator of the global DNA damage response. Immunofluorescence microscopy of cells  
308 expressing NmeCas9 or dNmeCas9 exhibited no increase in  $\gamma$ H2AX foci compared to wildtype E14,  
309 suggesting that sustained NmeCas9 expression is not genotoxic (Supplemental Fig. 2A). In contrast, cells  
310 exposed to UV light showed a significant increase in  $\gamma$ H2AX levels. Flow cytometric measurements of  
311  $\gamma$ H2AX immunostaining confirmed these results (Supplemental Fig. 2B). These data suggest that  
312 NmeCas9 expression does not lead to a global DNA damage response in mESCs.

313

314 **Comparative analysis of NmeCas9 and SpyCas9**

315 SpyCas9 is by far the best-characterized Cas9 orthologue, and is therefore the most informative  
316 benchmark when defining the efficiency and accuracy of other Cas9s. To facilitate comparative  
317 experiments between NmeCas9 and SpyCas9, we developed a matched Cas9 + sgRNA expression system  
318 for the two orthologs. This serves to minimize the expression differences between the two Cas9s in our

319 comparative experiments, beyond those differences dictated by the sequence variations between the  
320 orthologues themselves. To this end, we employed the separate pCSDest2-SpyCas9-NLS-3XHA-NLS  
321 (Addgene #69220) and pLKO.1-puro-U6sgRNA-BfuA1 (Addgene #52628) plasmids reported previously  
322 for the expression of SpyCas9 (driven by the CMV promoter) and its sgRNA (driven by the U6 promoter),  
323 respectively [58, 65]. We then replaced the bacterially-derived SpyCas9 sequence (i.e., not including the  
324 terminal fusions) with that of NmeCas9 in the CMV-driven expression plasmid. This yielded an  
325 NmeCas9 expression vector (pEJS424) that is identical to that of the SpyCas9 expression vector in every  
326 way (backbone, promoters, UTRs, poly(A) signals, terminal fusions, etc.) except for the Cas9 sequence  
327 itself. Similarly, we replaced the SpyCas9 sgRNA cassette in pLKO.1-puro-U6sgRNA-BfuA1 with that of  
328 the NmeCas9 sgRNA [46, 53], yielding the NmeCas9 sgRNA expression plasmid pEJS333. This matched  
329 system facilitates direct comparisons of the two enzymes' accumulation and activity during editing  
330 experiments. To assess relative expression levels of the identically-tagged Cas9 orthologs, the two plasmids  
331 were transiently transfected into HEK293T cells for 48 hours, and the expression of the two proteins was  
332 monitored by anti-HA western blot (Fig. 4A). Consistent with our previous data (Fig. 1A), analyses of  
333 samples from identically transfected cells show that NmeCas9 accumulation is stronger when co-expressed  
334 with its cognate sgRNA (Fig. 4A, compare lane 6 to 4 and 5), whereas SpyCas9 is not affected by the  
335 presence of its sgRNA (lanes 1-3).

336 For an initial comparison of the cleavage efficiencies of the two Cas9s, we chose three previously  
337 validated SpyCas9 guides targeting the *AAVS1* "safe harbor" locus [20, 75] and used the CRISPRseek  
338 package [76] to design three NmeCas9 guides targeting the same locus within a region of ~700 base pairs  
339 (Supplemental Fig. 3A). The matched Cas9/sgRNA expression systems described above were used for  
340 transient transfection of HEK293T cells. T7E1 analysis showed that the editing efficiencies were  
341 comparable, with the highest efficiency being observed when targeting the NTS59 site with NmeCas9  
342 (Fig. 4B and Supplemental Fig. 3B).

343 To provide a direct comparison of editing efficiency between the SpyCas9 and NmeCas9 systems,  
344 we took advantage of the non-overlapping PAMs of SpyCas9 and NmeCas9 (NGG and N<sub>4</sub>GATT,

345 respectively). Because the optimal SpyCas9 and NmeCas9 PAMs are non-overlapping, it is simple to  
346 identify chromosomal target sites that are compatible with both orthologues, i.e. that are dual target sites  
347 (DTSs) with a composite PAM sequence of NGGNGATT that is preferred by both nucleases. In this  
348 sequence context, both Cas9s will cleave the exact same internucleotide bond (**NN/NNNNGGNGATT**;  
349 cleaved junction in bold, and PAM region underlined), and both Cas9s will have to contend with the  
350 exact same sequence and chromatin structural context. Furthermore, if the target site contains a G residue  
351 at position -24 of the sgRNA-noncomplementary strand (relative to the PAM) and another at position -20,  
352 then the U6 promoter can be used to express perfectly-matched sgRNAs for both Cas9 orthologues. Four  
353 DTSs with these characteristics were used in this comparison (Supplemental Fig. 4A). We had previously  
354 used NmeCas9 to target a site (NTS7) that happened also to match the SpyCas9 PAM consensus, so we  
355 included it in our comparative analysis as a fifth site, even though it has a predicted rG-dT wobble pair at  
356 position -24 for the NmeCas9 sgRNA (Supplemental Fig. 4A).

357 We set out next to compare the editing activities of both Cas9 orthologs programmed to target the  
358 five chromosomal sites depicted in Supplemental Fig. 4A, initially via T7E1 digestion. SpyCas9 was more  
359 efficient than NmeCas9 at generating lesions at the DTS1 and DTS8 sites (Fig. 4C, lanes 1-2 and 13-14).  
360 In contrast, NmeCas9 was more efficient than SpyCas9 at the DTS3 and NTS7 sites (Fig. 4C, lanes 5-6  
361 and 17-18). Editing at DTS7 was approximately equal with both orthologs (Fig. 4C, lanes 9-10). Data  
362 from three biological replicates of all five target sites are plotted in Fig. 4D. The remainder of our  
363 comparative studies focused on DTS3, DTS7, and DTS8, as they provided examples of target sites with  
364 NmeCas9 editing efficiencies that are greater than, equal to, or lower than those of SpyCas9, respectively.  
365 At all three of these sites, the addition of an extra 5'-terminal G residue had little to no effect on editing by  
366 either SpyCas9 or NmeCas9 (Supplemental Fig. 4B). Truncation of the three NmeCas9 guides down to  
367 20 nucleotides (all perfectly matched) again had differential effects on editing efficiency from one site to  
368 the next, with no reduction in DTS7 editing, partial reduction in DTS3 editing, and complete loss of  
369 DTS8 editing (Supplemental Fig. 4B).

370

371 **Assessing the genome-wide precision of NmeCas9 editing**

372 All Cas9 orthologs described to date have some propensity to edit off-target sites lacking perfect  
373 complementarity to the programmed guide RNA, and considerable effort has been devoted to developing  
374 strategies (mostly with SpyCas9) to increase editing specificity (reviewed in [31, 34, 35]). In comparison  
375 with SpyCas9, orthologs such as NmeCas9 that employ longer guide sequences and that require longer  
376 PAMs have the potential for greater on-target specificity, possibly due in part to the lower density of near-  
377 cognate sequences. As an initial step in exploring this possibility, we used CRISPRseek [76] to perform a  
378 global analysis of potential NmeCas9 and SpyCas9 off-target sites with six or fewer mismatches in the  
379 human genome, using sgRNAs specific for DTS3, DTS7 and DTS8 (Fig. 5A) as representative queries.  
380 When allowing for permissive and semi-permissive PAMs (NGG, NGA, and NAG for SpyCas9;  
381 N<sub>4</sub>GHTT, N<sub>4</sub>GACT, N<sub>4</sub>GAYA, and N<sub>4</sub>GTCT for NmeCas9), potential off-target sites for NmeCas9  
382 were predicted with two to three orders of magnitude lower frequency than for SpyCas9 (Table 2).  
383 Furthermore, NmeCas9 off-target sites with fewer than five mismatches were rare (two sites with four

Number of mismatches	SpyCas9 sites (NGG, NGA, NAG PAMs)			NmeCas9 sites (N <sub>4</sub> GATT, N <sub>4</sub> GCTT, N <sub>4</sub> GTAA, N <sub>4</sub> GATA, N <sub>4</sub> GTCT, N <sub>4</sub> GACA PAMs)		
	DTS3	DTS7	DTS8	DTS3	DTS7	DTS8
1	0	0	0	0	0	0
2	4	2	2	0	0	0
3	45	52	60	0	0	0
4	680	500	772	0	2	0
5	6,691	4,116	7,325	4	5	25
6	45,897	26,474	52,547	17	61	129
<b>Total</b>	<b>53,317</b>	<b>31,144</b>	<b>60,706</b>	<b>21</b>	<b>68</b>	<b>154</b>

384 **Table 2.** Number of predicted near-cognate sites in the human genome for the three dual target sites (DTS3, DTS7  
385 and DTS8) analyzed in this study. These potential off-target sites differ from the on-target site by six or fewer  
386 mismatches, as listed on the left, and include the functional or semi-functional PAMs shown at the top.

387 mismatches) for DTS7, and non-existent for DTS3 and DTS8 (Table 2). Even when we relaxed the  
388 NmeCas9 PAM requirement to N<sub>4</sub>GN<sub>3</sub>, which includes some PAMs that enable only background levels of  
389 targeting (e.g. N<sub>4</sub>GATC (Fig. 3A)), the vast majority of predicted off-target sites (>96%) for these three  
390 guides had five or more mismatches, and none had fewer than four mismatches (Fig. 5A). In contrast, the  
391 SpyCas9 guides targeting DTS3, DTS7, and DTS8 had 49, 54, and 62 predicted off-target sites with

392 three or fewer mismatches, respectively (Table 2). As speculated previously [53, 54], these bioinformatic  
393 predictions suggest the intriguing possibility that the NmeCas9 genome editing system may induce very  
394 few undesired mutations, or perhaps none, even when targeting sites that induce substantial off-targeting  
395 with SpyCas9.

396         Although bioinformatic predictions of off-targeting can be useful, it is well established that off-  
397 target profiles must be defined experimentally in a prediction-independent fashion due to our limited  
398 understanding of target specificity determinants, and the corresponding inability of algorithms to predict  
399 all possible sites successfully [31, 34, 35]. The need for empirical off-target profiling is especially acute  
400 with Cas9 orthologs that are far less thoroughly characterized than SpyCas9. A previous report used PCR  
401 amplification and high-throughput sequencing to detect the frequencies of lesions at 15-20 predicted  
402 NmeCas9 off-target sites for each of three guides in human cells, and found only background levels of  
403 indels in all cases, suggesting a very high degree of precision for NmeCas9 [54]. However, this report  
404 restricted its analysis to candidate sites with N<sub>4</sub>GNTT PAMs and three or fewer mismatches (or two  
405 mismatches combined with a 1-nt bulge) in the PAM-proximal 19 nucleotides, leaving open the possibility  
406 that legitimate off-target sites that did not fit these specific criteria remained unexamined. Accordingly,  
407 empirical and minimally-biased off-target profiles have never been generated for any NmeCas9/sgRNA  
408 combination, and the true off-target propensity of NmeCas9 therefore remains unknown. At the time we  
409 began this work, multiple methods for prediction-independent detection of off-target sites had been  
410 reported including GUIDE-seq, BLESS, Digenome-Seq, HTGTS, and IDLV capture, each with their  
411 own advantages and disadvantages (reviewed in [31, 34, 35]); additional methods (SITE-Seq [64],  
412 CIRCLE-seq [77], and BLISS [78]) have been reported more recently. Initially we chose to apply  
413 GUIDE-seq [63], which takes advantage of oligonucleotide incorporation into double-strand break sites,  
414 for defining the off-target profiles of both SpyCas9 and NmeCas9 when each is programmed to edit the  
415 DTS3, DTS7 and DTS8 sites (Fig. 4C-D) in the human genome.

416         After confirming that the co-transfected double-stranded oligodeoxynucleotide (dsODN) was  
417 incorporated efficiently at the DTS3, DTS7 and DTS8 sites during both NmeCas9 and SpyCas9 editing

418 (Supplemental Fig. 4C), we then prepared GUIDE-seq libraries for each of the six editing conditions, as  
419 well as for the negative control conditions (i.e., in the absence of any sgRNA) for both Cas9 orthologs.  
420 The GUIDE-seq libraries were then subjected to high-throughput sequencing, mapped, and analyzed as  
421 described [79] (Fig. 5B-C). On-target editing with these guides was readily detected by this method, with  
422 the number of independent reads ranging from a low of 167 (NmeCas9, DTS8) to a high of 1,834  
423 (NmeCas9, DTS3) (Fig. 5C and Supplemental Table 2).

424 For our initial analyses, we scored candidate sites as true off-targets if they yielded two or more  
425 independent reads and had six or fewer mismatches with the guide, with no constraints placed on the  
426 PAM match at that site. For SpyCas9, two of the sgRNAs (targeting DTS3 and DTS7) induced  
427 substantial numbers of off-target editing events (271 and 54 off-target sites, respectively (Fig. 5B)) under  
428 these criteria. The majority of these SpyCas9 off-target sites (88% and 77% for DTS3 and DTS7,  
429 respectively) were associated with a canonical NGG PAM. Reads were very abundant at many of these  
430 loci, and at five off-target sites (all with the DTS3 sgRNA) even exceeded the number of on-target reads  
431 (Fig. 5C). SpyCas9 was much more precise with the DTS8 sgRNA: we detected a single off-target site  
432 with five mismatches and an NGG PAM, and it was associated with only three independent reads, far  
433 lower than the 415 reads that we detected at the on-target site (Fig. 5C and Supplemental Table 2).  
434 Overall, the range of editing accuracies that we measured empirically for SpyCas9 – very high (e.g.  
435 DTS8), intermediate (e.g. DTS7), and poor (e.g. DTS3) – are consistent with the observations of other  
436 reports using distinct guides (reviewed in [31, 34, 35]).

437 In striking contrast, GUIDE-seq analyses with NmeCas9, programmed with sgRNAs targeting  
438 the exact same three sites, yielded off-target profiles that were exceptionally specific in all cases (Fig. 5B-  
439 C). For DTS3 and DTS8 we found no reads at any site with six or fewer guide mismatches; for DTS7 we  
440 found one off-target site with four mismatches (three of which were at the PAM-distal end; see  
441 Supplemental Table 2), and even at this site there were only 12 independent reads, ~100x fewer than the  
442 1,222 reads detected at DTS7 itself. This off-target site was also associated with a PAM (N<sub>4</sub>GGCT) that  
443 would be expected to be poorly functional, though it could also be considered a “slipped” PAM with a

444 more optimal consensus but variant spacing (N<sub>5</sub>GCTT). Purified, recombinant NmeCas9 has been  
445 observed to catalyze DNA cleavage *in vitro* at a site with a similarly slipped PAM [52]. To explore the off-  
446 targeting potential of NmeCas9 further, we decreased the stringency of our mapping to allow detection of  
447 off-target sites with up to 10 mismatches. Even in these conditions, only four (DTS7), 15 (DTS8), and 16  
448 (DTS3) candidate sites were identified, most of which had only four or fewer reads (Fig. 5C) and were  
449 associated with poorly functional PAMs (Supplemental Table 2). We consider it likely that most if not all  
450 of these low-probability candidate off-target sites represent background noise caused by spurious priming  
451 and other sources of experimental error.

452 As an additional test of off-targeting potential, we repeated the DTS7 GUIDE-seq experiments  
453 with both SpyCas9 and NmeCas9, but this time using a different transfection reagent (Lipofectamine3000  
454 rather than Polyfect). These repeat experiments revealed that >96% (29 out of 30) of off-target sites with  
455 up to five mismatches were detected under both transfection conditions for SpyCas9 (Supplemental Table  
456 1). However, the NmeCas9 GUIDE-seq data showed no overlap between the potential sites identified  
457 under the two conditions, again suggesting that the few off-target reads that we did observe are unlikely to  
458 represent legitimate off-target editing sites.

459 To confirm the validity of the off-target sites defined by GUIDE-seq, we designed primers  
460 flanking candidate off-target sites identified by GUIDE-seq, PCR-amplified those loci following standard  
461 genome editing (i.e., in the absence of co-transfected GUIDE-seq dsODN) (3 biological replicates), and  
462 then subjected the PCR products to high-throughput sequencing to detect the frequencies of Cas9-  
463 induced indels. For this analysis we chose the top candidate off-target sites (as defined by GUIDE-seq read  
464 count) for each of the six cases (DTS3, DTS7 and DTS8, each edited by either SpyCas9 or NmeCas9). In  
465 addition, due to the low numbers of off-target sites and the low off-target read counts observed during the  
466 NmeCas9 GUIDE-seq experiments, we analyzed the top two predicted off-target sites for the three  
467 NmeCas9 sgRNAs, as identified by CRISPRseek (Fig. 5A and Table 2) [76]. On-target indel formation  
468 was detected in all cases, with editing efficiencies ranging from 7% (DTS8, with both SpyCas9 and  
469 NmeCas9) to 39% (DTS3 with NmeCas9) (Fig. 5D). At the off-target sites, our targeted deep-sequencing

470 analyses largely confirmed our GUIDE-seq results: SpyCas9 readily induced indels at most of the tested  
471 off-target sites when paired with the DTS3 and DTS7 sgRNAs, and in some cases the off-target editing  
472 efficiencies approached those observed at the on-target sites (Fig. 5D). Although some SpyCas9 off-  
473 targeting could also be detected with the DTS8 sgRNA, the frequencies were much lower (<0.1% in all  
474 cases). Off-target lesions induced by NmeCas9 were far less frequent in all cases, even with the DTS3  
475 sgRNA that was so efficient at on-target mutagenesis: many off-target sites exhibited lesion efficiencies  
476 that were indistinguishable from background, and never rose above ~0.02% (Fig. 5D). These results, in  
477 combination with the GUIDE-seq analyses described above, reveal wild-type NmeCas9 to be an  
478 exceptionally precise genome editing enzyme.

479 To explore NmeCas9 editing accuracy more deeply, we chose 16 additional NmeCas9 target sites  
480 across the genome, 10 with canonical N<sub>4</sub>GATT PAMs and six with variant functional PAMs  
481 (Supplemental Table 9). We then performed GUIDE-seq and analyses of NmeCas9 editing at these sites.  
482 GUIDE-seq analysis readily revealed editing at each of these sites, with on-target read counts ranging  
483 from ~100 to ~5,000 reads (Fig. 6A). More notably, off-target reads were undetectable by GUIDE-seq  
484 with 14 out of the 16 sgRNAs (Fig. 6B). Targeted deep sequencing of PCR amplicons, which is a more  
485 quantitative readout of editing efficiency than either GUIDE-seq or T7E1 analysis, confirmed on-target  
486 editing in all cases, with indel efficiencies ranging from ~5-85% (Fig. 6C).

487 The two guides with off-target activity (NTS1C and NTS25) had only two and one off-target sites,  
488 respectively (Fig. 6B and Supplemental Fig. 5). Off-target editing was confirmed by high-throughput  
489 sequencing and analysis of indels (Fig. 6D). Compared with the on-target site (perfectly matched at all  
490 positions other than the 5'-terminal guide nucleotide, and with an optimal N<sub>4</sub>GATT PAM), the efficiently  
491 targeted NTS1C-OT1 had two wobble pairs and one mismatch (all in the nine PAM-distal nucleotides),  
492 as well as a canonical N<sub>4</sub>GATT PAM (Fig. 6E and Supplemental Table 2). The weakly edited NTS1C-  
493 OT2 site had only a single mismatch (at the 11<sup>th</sup> nucleotide, counting in the PAM-distal direction), but  
494 was associated with a non-canonical N<sub>4</sub>GGTT (or a “slipped” N<sub>5</sub>GTTT) PAM (Fig. 6E and  
495 Supplemental Table 2). NTS25 with an N<sub>4</sub>GATA PAM was the other guide with a single off-target site

496 (NTS25-OT1), where NmeCas9 cleaved and edited up to ~1,000x less efficiently than at the on-target site  
497 (Fig. 6D). This minimal amount of off-target editing arose despite the association of NTS25-OT1 with an  
498 optimal N<sub>4</sub>GATT PAM, unlike the variant N<sub>4</sub>GATA PAM that flanks the on-target site. Overall, our  
499 GUIDE-seq and sequencing-based analyses demonstrate that NmeCas9 genome editing is exceptionally  
500 accurate: we detected and confirmed cellular off-target editing with only two of the 19 guides tested, and  
501 even in those two cases, only one or two off-target sites could be found for each. Furthermore, of the three  
502 bona fide off-target sites that we identified, only one generated indels at substantial frequency (11.6%);  
503 indel frequencies were very modest (0.3% or lower) at the other two off-target sites.

504 We next sought to corroborate and expand on our GUIDE-seq results with a second prediction-  
505 independent method. We applied the SITE-Seq<sup>TM</sup> (Caribou Biosciences, Inc., Berkeley, CA) assay, a  
506 biochemical-based method that does not rely on cellular events such as DNA repair, thus potentially  
507 enabling a more thorough profiling of genome-wide specificity [63]. SITE-Seq libraries were prepared for  
508 the three dual target sites with both Cas9 orthologues as well as for twelve of the NmeCas9-only target  
509 sites. SITE-Seq was performed on HEK293T genomic DNA (gDNA) treated with a range of RNP  
510 concentrations (4 nM – 256 nM) previously shown to discriminate high and low probability cellular off-  
511 targets [63]. Finally, the resulting libraries were sequenced, aligned, and then analyzed as previously  
512 described [63].

513 Negative controls without RNP recovered zero sites across any concentrations, whereas SpyCas9  
514 assembled with sgRNAs targeting DTS3, DTS7, or DTS8 recovered hundreds (at 4 nM RNP) to  
515 thousands (at 256 nM RNP) of biochemical off-target sites (Fig. 6F). In contrast, NmeCas9 assembled  
516 with sgRNAs targeting the same three sites recovered only their on-target sites at 4 nM RNP and at most  
517 29 off-target sites at 256 nM RNP (Fig. 6F). Moreover, the 12 additional NmeCas9 target sites showed  
518 similarly high specificity: eight samples recovered only the on-target sites at 4 nM RNP and six of those  
519 recovered no more than nine off-targets at 256 nM RNP (Supplemental Fig. 6A). Across NmeCas9  
520 RNPs, off-target sequence mismatches appeared enriched in the 5' end of the sgRNA target sequence  
521 (Supplemental Table 4). Finally, three of the NmeCas9 RNPs (NTS30, NTS4C, and NTS59) required

522 elevated concentrations to retrieve their on-targets, potentially due to poor sgRNA transcription and/or  
523 RNP assembly. These RNPs were therefore excluded from further analysis.

524 We next performed cell-based validation experiments to investigate whether any of the  
525 biochemical off-targets were edited in cells. Since NmeCas9 recovered only ~100 biochemical off-targets  
526 across all RNPs and concentrations, we could examine each site for editing in cells. SpyCas9 generated  
527 >10,000 biochemical off-targets across all DTS samples, preventing comprehensive cellular profiling.  
528 Therefore, for each RNP we selected 96 of the high cleavage sensitivity SITE-Seq sites (i.e., recovered at  
529 all concentrations tested in SITE-Seq) for examination, as we predicted those were more likely to  
530 accumulate edits in cells [63] (Supplemental Table 5). Sites were randomly selected within this cohort  
531 and only included a subset of the GUIDE-seq validation test set sites (1/8 and 5/8 overlapping sites for  
532 DTS3 and DTS7, respectively). Additionally, SITE-Seq and GUIDE-seq validations were performed on  
533 the same gDNA samples to facilitate comparisons between data sets.

534 Across all NmeCas9 RNPs, only three cellular off-targets were observed. These three all  
535 belonged to the NTS1C RNP, and two of them had also been detected with GUIDE-seq. Of note, all  
536 high cleavage sensitivity SITE-Seq sites (i.e., all on-targets and the single prominent NTS1C off-target,  
537 NTS1C-OT1) showed editing in cells. Conversely, SITE-Seq sites with low cleavage sensitivity, defined  
538 as being recovered at only 64 nM and/or 256 nM RNP, were rarely found as edited (2/93 sites).  
539 Importantly, this suggests that we identified all or the clear majority of NmeCas9 cellular off-targets, albeit  
540 at our limit of detection. Across all SpyCas9 RNPs, 14 cellular off-targets were observed (8/70 sites for  
541 DTS3, 6/83 sites for DTS7, and 0/79 sites for DTS8) (Supplemental Table 5). Since our data set was  
542 only a subset of the total number of high cleavage sensitivity SITE-Seq sites, and excluded many of the  
543 GUIDE-seq validated sites, we expect that sequencing all SITE-Seq sites would uncover additional  
544 cellular off-targets. Taken together, these data corroborate our GUIDE-seq results, suggesting that  
545 NmeCas9 can serve as a highly specific genome editing platform.

546

547 **Indel spectrum at NmeCas9-edited sites**

548 Our targeted deep sequencing data at the three dual target sites (Fig. 5D, Supplemental Fig. 4A  
549 and Supplemental Table 5) enabled us to analyze the spectrum of insertions and deletions generated by  
550 NmeCas9, in comparison with those of SpyCas9 when editing the exact same sites (Supplemental Figs. 6B  
551 and 7-9). Although small deletions predominated at all three sites with both Cas9 orthologs, the frequency  
552 of insertions was lower for NmeCas9 than it was with SpyCas9 (Supplemental Figs. 6B and 7-9). For both  
553 SpyCas9 and NmeCas9, the vast majority of insertions were only a single nucleotide (Supplemental Fig.  
554 8). The sizes of the deletions varied from one target site to the other for both Cas9 orthologs. Our data  
555 suggest that at Cas9 edits, deletions predominated over insertions and the indel size varies considerably  
556 site to site (Supplemental Figs. 6B, 10 and 11).

557

### 558 **Truncated sgRNAs reduce off-target cleavage by NmeCas9**

559 Although NmeCas9 exhibits very little propensity to edit off-target sites, for therapeutic  
560 applications it may be desirable to suppress even the small amount of off-targeting that occurs (Fig. 6).  
561 Several strategies have been developed to suppress off-targeting by SpyCas9 [31, 34, 35], some of which  
562 could be readily applied to other orthologs. For example, truncated sgRNAs (tru-sgRNAs) sometimes  
563 suppress off-target SpyCas9 editing more than they suppress on-target editing [69]. Because 5'-terminal  
564 truncations are compatible with NmeCas9 function (Fig. 2), we tested whether NmeCas9 tru-sgRNAs can  
565 have similar suppressive effects on off-target editing without sacrificing on-target editing efficiency.

566 First, we tested whether guide truncation can lead to NmeCas9 editing at novel off-target sites (i.e.  
567 at off-target sites not edited by full-length guides), as reported previously for SpyCas9 [69]. Our earlier  
568 tests of NmeCas9 on-target editing with tru-sgRNAs used guides targeting the NTS33 (Fig. 2B-C) and  
569 NTS32 (Fig. 2D-E) sites. GUIDE-seq did not detect any NmeCas9 off-target sites during editing with full-  
570 length NTS32 and NTS33 sgRNAs (Fig. 6). We again used GUIDE-seq with a subset of the validated  
571 NTS32 and NTS33 tru-sgRNAs to determine whether NmeCas9 guide truncation leads to off-target  
572 editing at new sites, and found none (Supplemental Fig. 12). Although we cannot rule out the possibility

573 that other NmeCas9 guides could be identified that yield novel off-target events upon truncation, our  
574 results suggest that *de novo* off-targeting by NmeCas9 tru-sgRNAs is unlikely to be a pervasive problem.

575 The most efficiently edited off-target site from our previous analyses was NTS1C-OT1, providing  
576 us with our most stringent test of off-target suppression. When targeted by the NTS1C sgRNA, NTS1C-  
577 OT1 has one rG-dT wobble pair at position -16 (i.e., at the 16<sup>th</sup> base pair from the PAM-proximal end of  
578 the R-loop), one rC-dC mismatch at position -19, and one rU-dG wobble pair at position -23 (Fig. 6E).  
579 We generated a series of NTS1C-targeting sgRNAs with a single 5'-terminal G (for U6 promoter  
580 transcription) and spacer complementarities ranging from 24 to 15 nucleotides (GN<sub>24</sub> to GN<sub>15</sub>,  
581 Supplemental Fig. 13A, top panel). Conversely, we designed a similar series of sgRNAs with perfect  
582 complementarity to NTS1C-OT1 (Supplemental Fig. 13B, top panel). Consistent with our earlier results  
583 with other target sites (Fig. 2), T7E1 analyses revealed that both sets of guides enabled editing of the  
584 perfectly-matched on-target site with truncations down to 19 nucleotides (GN<sub>18</sub>), but that shorter guides  
585 were inactive. On-target editing efficiencies at both sites were comparable across the seven active guide  
586 lengths (GN<sub>24</sub> through GN<sub>18</sub>), with the exception of slightly lower efficiencies with the GN<sub>19</sub> guides  
587 (Supplemental Fig. 13A & B, middle and bottom panels).

588 We then used targeted deep sequencing to test whether off-target editing is reduced with the  
589 truncated sgRNAs. With both sets of sgRNAs (perfectly complementary to either NTS1C or NTS1C-  
590 OT1), we found that off-targeting at the corresponding near-cognate site persisted with the four longest  
591 guides (GN<sub>24</sub>, GN<sub>23</sub>, GN<sub>22</sub>, GN<sub>21</sub>; Fig. 7). However, off-targeting was abolished with the GN<sub>20</sub> guide,  
592 without any significant reduction in on-target editing efficiencies (Fig. 7). Off-targeting was also absent  
593 with the GN<sub>19</sub> guide, though on-target editing efficiency was compromised. These results, albeit from a  
594 limited data set, indicate that truncated sgRNAs (especially those with 20 or 19 base pairs of guide/target  
595 complementarity, 4-5 base pairs fewer than the natural length) can suppress even the limited degree of off-  
596 targeting that occurs with NmeCas9.

597 Unexpectedly, even though off-targeting at NTS1C-OT1 was abolished with the GN<sub>20</sub> and GN<sub>19</sub>  
598 truncated NTS1C sgRNAs, truncating by an additional nucleotide (to generate the GN<sub>18</sub> sgRNA) once

599 again yielded NTS1C-OT1 edits (Fig. 7A). This could be explained by the extra G residue at the 5'-  
600 terminus of each sgRNA in the truncation series (Supplemental Fig. 13). With the NTS1C GN<sub>19</sub> sgRNA,  
601 both the 5'-terminal G residue and the adjacent C residue are mismatched with the NTS1C-OT1 site. In  
602 contrast, with the GN<sub>18</sub> sgRNA, the 5'-terminal G is complementary to the off-target site. In other words,  
603 with the NTS1C GN<sub>19</sub> and GN<sub>18</sub> sgRNAs, the NTS1C-OT1 off-target interactions (which are identical in  
604 the PAM-proximal 17 nucleotides) include two additional nucleotides of non-complementarity or one  
605 additional nucleotide of complementarity, respectively. Thus, the more extensively truncated GN<sub>18</sub>  
606 sgRNA has *greater* complementarity with the NTS1C-OT1 site than the GN<sub>19</sub> sgRNA, explaining the re-  
607 emergence of off-target editing with the former. This observation highlights the fact that the inclusion of a  
608 5'-terminal G residue that is mismatched with the on-target site, but that is complementary to a C residue  
609 at an off-target site, can limit the effectiveness of a truncated guide at suppressing off-target editing,  
610 necessitating care in truncated sgRNA design when the sgRNA is generated by cellular transcription. This  
611 issue is not a concern with sgRNAs that are generated by other means (e.g. chemical synthesis) that do not  
612 require a 5'-terminal G. Overall, our results demonstrate that NmeCas9 genome editing is exceptionally  
613 precise, and even when rare off-target editing events occur, tru-sgRNAs can provide a simple and effective  
614 way to suppress them.

615

## 616 **DISCUSSION**

617 The ability to use Type II and Type V CRISPR-Cas systems as RNA-programmable DNA-  
618 cleaving systems [13, 14, 27] is revolutionizing many aspects of the life sciences, and holds similar promise  
619 for biotechnological, agricultural, and clinical applications. Most applications reported thus far have used  
620 a single Cas9 ortholog (SpyCas9). Thousands of additional Cas9 orthologs have also been identified [28],  
621 but only a few have been characterized, validated for genome engineering applications, or both. Adding  
622 additional orthologs promises to increase the number of targetable sites (through new PAM specificities),  
623 extend multiplexing possibilities (for pairwise combinations of Cas9 orthologs with orthogonal guides), and  
624 improve deliverability (for the more compact Cas9 orthologs). In addition, some Cas9s may show

625 mechanistic distinctions (such as staggered vs. blunt dsDNA breaks) [80], greater protein stability *in vivo*,  
626 improved control mechanisms (e.g. via multiple anti-CRISPRs that act at various stages of the DNA  
627 cleavage pathway) [57, 58, 60, 61, 81-83], and other enhancements. Finally, some may exhibit a greater  
628 natural propensity to distinguish between on- vs. off-target sites during genome editing applications,  
629 obviating the need for extensive engineering (as was necessary with SpyCas9) to attain the accuracy  
630 needed for many applications, especially therapeutic development.

631 Here we have further defined the properties of NmeCas9 during editing in human cells, including  
632 validation and extension of previous analyses of guide length and PAM requirements [46, 53, 54].

633 Intriguingly, the tolerance to deviations from the N<sub>4</sub>G(A/C)TT natural PAM consensus [51] observed *in*  
634 *vitro* and in bacterial cells [46, 52] is considerably reduced in the mammalian context, i.e. fewer PAM  
635 variations are permitted during mammalian editing. The basis for this context-dependent difference is not  
636 clear but may be due in part to the ability to access targets within eukaryotic chromatin, or to decreased  
637 expression levels relative to potential DNA substrates, since lower SpyCas9/sgRNA concentrations have  
638 been shown to improve accuracy [30, 84, 85]. We have also found that steady-state NmeCas9 levels in  
639 human cells are markedly increased in the presence of its cognate sgRNA, suggesting that sgRNA-loaded  
640 NmeCas9 is more stable than *apo* NmeCas9. An increased proteolytic sensitivity of *apo* Cas9 relative to the  
641 sgRNA-bound form has been noted previously for a different Type II-C ortholog (*Corynebacterium diphtheriae*  
642 Cas9, CdiCas9 [55]).

643 A previous report indicated that NmeCas9 has high intrinsic accuracy, based on analyses of  
644 candidate off-target sites that were predicted bioinformatically [54]. However, the true genome-wide  
645 accuracy of NmeCas9 was not assessed empirically, as is necessary given well-established imperfections in  
646 bioinformatic predictions of off-targeting [31, 34, 35]. We have used GUIDE-seq [63] and SITE-Seq [64]  
647 to define the genome-wide accuracy of wild-type NmeCas9, including side-by-side comparisons with  
648 wildtype SpyCas9 during editing of identical on-target sites. We find that NmeCas9 is a consistently high-  
649 accuracy genome editor, with off-target editing undetectable above background with 17 out of 19  
650 analyzed sgRNAs, and only one or three verified off-target edits with the remaining two guides. We

651 observed this exquisite specificity by NmeCas9 even with sgRNAs that target sites (DTS3 and DTS7 (see  
652 Fig. 5)) that are highly prone to off-target editing when targeted with SpyCas9. Of the four off-target sites  
653 that we validated, three accumulated <1% indels. Even with the one sgRNA that yielded a significant  
654 frequency of off-target editing (NTS1C, which induced indels at NTS1C-OT1 with approximately half  
655 the efficiency of on-target editing), the off-targeting with wild-type NmeCas9 could be easily suppressed  
656 with truncated sgRNAs. Our ability to detect NTS25-OT1 editing with GUIDE-seq, despite its very low  
657 (0.06%) editing efficiency based on high-throughput sequencing, indicates that our GUIDE-seq  
658 experiments can identify even very low-efficiency off-target editing sites. Similar considerations apply to  
659 our SITE-Seq analyses. We observed high accuracy even when NmeCas9 is delivered by plasmid  
660 transfection, a delivery method that is associated with higher off-target editing than more transient  
661 delivery modes such as RNP delivery [86, 87].

662 The two Type II-C Cas9 orthologs (NmeCas9 and CjeCas9) that have been validated for  
663 mammalian genome editing and assessed for genome-wide specificity [47, 54] (this work) have both  
664 proven to be naturally hyper-accurate. Both use longer guide sequences than the 20-nucleotide guides  
665 employed by SpyCas9, and both also have longer and more restrictive PAM requirements. For both Type  
666 II-C orthologs, it is not yet known whether the longer PAMs, longer guides, or both account for the  
667 limited off-target editing. Type II-C Cas9 orthologs generally cleave dsDNA more slowly than SpyCas9  
668 [49, 55], and it has been noted that lowering  $k_{cat}$  can, in some circumstances, enhance specificity [88].  
669 Whatever the mechanistic basis for the high intrinsic accuracy, it is noteworthy that it is a property of the  
670 native proteins, without a requirement for extensive engineering. This adds to the motivation to identify  
671 more Cas9 orthologs with human genome editing activity, as it suggests that it may be unnecessary in  
672 many cases (perhaps especially among Type II-C enzymes) to invest heavily in structural and mechanistic  
673 analyses and engineering efforts to attain sufficient accuracy for many applications and with many desired  
674 guides, as was done with (for example) SpyCas9 [32, 33, 37, 38, 65]. Although Cas9 orthologs with more  
675 restrictive PAM requirements (such as NmeCas9, CjeCas9, and GeoCas9) by definition will afford lower  
676 densities of potential target sites than SpyCas9 (which also usually affords the highest on-target editing

677 efficiencies among established Cas9 orthologs), the combined targeting possibilities for multiple such  
678 Cas9s will increase the targeting options available within a desired sequence window, with little propensity  
679 for off-targeting. The continued exploration of natural Cas9 variation, especially for those orthologs with  
680 other advantages such as small size and anti-CRISPR off-switch control, therefore has great potential to  
681 advance the CRISPR genome editing revolution.

682

## 683 **CONCLUSIONS**

684 NmeCas9 is an intrinsically high-accuracy genome editing enzyme in mammalian cells, and the limited  
685 off-target editing that occurs can (at least in some cases) be suppressed by guide truncation. Continued  
686 exploration of Cas9 orthologs could therefore yield additional enzymes that do not require extensive  
687 characterization and engineering to prevent off-target editing.

688

## 689 **METHODS**

### 690 **Plasmids**

691 Two plasmids for the expression of NmeCas9 were used in this study. The first construct (used in Figs. 1  
692 and 2) was derived from the plasmid pSimpleII where NmeCas9 was cloned under the control of the  
693 elongation factor-1 $\alpha$  promoter, as described previously [53]. The *Cas9* gene in this construct expresses a  
694 protein with two NLSs and an HA tag. To make an all-in-one expression plasmid, a fragment containing  
695 a *BsmBI*-crRNA cassette linked to the tracrRNA by six nucleotides, under the control of U6 RNA  
696 polymerase III promoter, was synthesized as a gene block (Integrated DNA Technologies) and inserted  
697 into pSimpleII, generating the pSimpleII-Cas9-sgRNA-*BsmBI* plasmid that includes all elements needed  
698 for editing. To insert specific spacer sequence into the crRNA cassette, synthetic oligonucleotides were  
699 annealed to generate a duplex with overhangs compatible with those generated by *BsmBI* digestion of the  
700 pSimpleII-Cas9-sgRNA-*BsmBI* plasmid. The insert was then ligated into the *BsmBI*-digested plasmid. For  
701 Figs. 3-7, NmeCas9 and SpyCas9 constructs were expressed from the pCS2-Dest Gateway plasmid under  
702 the control of the CMV IE94 promoter [89]. All sgRNAs used with pCS2-Dest-Cas9 were driven by the

703 U6 promoter in pLKO.1-puro [90]. The M427 GFP reporter plasmid [66] was used as described [65].

704

705 **Cell culture, transfection, and transduction**

706 HEK293T were cultured in DMEM with 10% FBS and 1% Penicillin/Streptomycin (Gibco) in a 37°C

707 incubator with 5% CO<sub>2</sub>. K562 cells were grown in the same conditions but using IMDM. HFF cells were

708 grown in the same conditions but using DMEM with Glutamax and 20% FBS without antibiotics. mESCs

709 were grown in DMEM supplemented with 10% FBS, glutamine beta-ME and LIF. For transient

710 transfection, we used early to mid-passage cells (passage number 4-18). Approximately 1.5 x 10<sup>5</sup> cells were

711 transfected with 150 ng Cas9-expressing plasmid, 150 ng sgRNA-expressing plasmid and 10 ng mCherry

712 plasmid using Polyfect transfection reagent (Qiagen) in a 24-well plate according to the manufacturer's

713 protocol. For the GFP reporter assay, 100 ng M427 plasmid was included in the co-transfection mix.

714 Transduction was done as described previously [91].

715

716 **Western blotting**

717 48 h after transfection, cells were harvested and lysed with 50 µl of RIPA buffer. Protein concentration

718 was determined with the BCA kit (Thermo Scientific) and 12 µg of proteins were used for electrophoresis

719 and blotting. The blots were probed with anti-HA (Sigma, H3663) and anti-GAPDH (Abcam, ab9485) as

720 primary antibodies, and then with horseradish peroxidase-conjugated anti-mouse IgG (Thermoscientific,

721 62-6520) or anti-rabbit IgG (Biorad, 1706515) secondary antibodies, respectively. Blots were visualized

722 using the Clarity Western ECL substrate (Biorad, 170-5060).

723 **Flow cytometry**

724 The GFP reporter was used as described previously [65]. Briefly, cells were harvested 48 hours after

725 transfection and used for FACS analysis (BD Accuri 6C). To minimize the effects of differences in the

726 efficiency of transfection among samples, cells were initially gated for mCherry-expression, and the

727 percentage of GFP-expressing cells were quantified within mCherry positive cells. All experiments were

728 performed in triplicate with data reported as mean values with error bars indicating the standard error of  
729 the mean (s.e.m.).

730 **Genome editing**

731 72 hours after transfection, genomic DNA was extracted via the DNeasy Blood and Tissue kit (Qiagen),  
732 according to the manufacturer's protocol. 50 ng DNA was used for PCR-amplification using primers  
733 specific for each genomic site (Supplemental Table 9) with High Fidelity 2X PCR Master Mix (New  
734 England Biolabs). For T7E1 analysis, 10  $\mu$ l of PCR product was hybridized and treated with 0.5  $\mu$ l T7  
735 Endonuclease I (10 U/ $\mu$ l, New England Biolabs) in 1X NEB Buffer 2 for 1 hour. Samples were run on a  
736 2.5% agarose gel, stained with SYBR-safe (ThermoFisher Scientific), and quantified using the  
737 ImageMaster-TotalLab program. Indel percentages are calculated as previously described [92, 93].  
738 Experiments for T7E1 analysis are performed in triplicate with data reported as mean  $\pm$  s.e.m. For indel  
739 analysis by TIDE, 20 ng of PCR product is purified and then sequenced by Sanger sequencing. The trace  
740 files were subjected to analysis using the TIDE web tool (<https://tide.deskgen.com>).  
741

742 **Expression and purification of NmeCas9**

743 NmeCas9 was cloned into the pMCSG7 vector containing a T7 promoter followed by a 6xHis tag and a  
744 tobacco etch virus (TEV) protease cleavage site. Two NLSs on the C-terminus of NmeCas9 and another  
745 NLS on the N-terminus were also incorporated. This construct was transformed into the Rosetta 2 DE3  
746 strain of *E. coli*. Expression of NmeCas9 was performed as previously described for SpyCas9 [14]. Briefly,  
747 a bacterial culture was grown at 37°C until an OD600 of 0.6 was reached. At this point the temperature  
748 was lowered to 18°C followed by addition of 1 mM Isopropyl  $\beta$ -D-1-thiogalactopyranoside (IPTG) to  
749 induce protein expression. Cells were grown overnight, and then harvested for purification. Purification of  
750 NmeCas9 was performed in three steps: Nickel affinity chromatography, cation exchange  
751 chromatography, and size exclusion chromatography. The detailed protocols for these can be found in  
752 [14].

753

754 **RNP delivery of NmeCas9**

755 RNP delivery of NmeCas9 was performed using the Neon transfection system (ThermoFisher).

756 Approximately 40 picomoles of NmeCas9 and 50 picomoles of sgRNA were mixed in buffer R and

757 incubated at room temperature for 30 minutes. This preassembled complex was then mixed with 50,000 –

758 150,000 cells, and electroporated using 10  $\mu$ L Neon tips. After electroporation, cells were plated in pre-

759 warmed 24-well plates containing the appropriate culture media without antibiotics. The number of cells

760 used and pulse parameters of electroporation were different for different cell types tested. The number of

761 cells used were 50,000, 100,000, and 150,000 for PLB985 cells, HEK293T cells, and K562/HFF cells

762 respectively. Electroporation parameters (voltage, width, number of pulses) were 1150 v, 20 ms, 2 pulses

763 for HEK293T cells; 1000 v, 50 ms, 1 pulse for K562 cells; 1350 v, 35 ms, 1 pulse for PLB985 cells; and

764 1700 v, 20 ms, 1pulse for HFF cells.

765

766  **$\gamma$ H2AX immunofluorescence staining and flow cytometry**

767 For immunofluorescence, mouse embryonic stem cells (mESCs) were crosslinked with 4%

768 paraformaldehyde and stained with anti- $\gamma$ H2AX (LP BIO, AR-0149-200) as primary antibody and Alexa

769 Fluor® 488 goat anti-rabbit IgG (Invitrogen, A11034) as secondary antibody. DNA was stained with

770 DAPI. For a positive control, E14 cells were irradiated with 254 nm UV light (3 mJ/cm<sup>2</sup>). Images were

771 taken by a Nikon Eclipse E400 and representative examples were chosen.

772 For flow cytometry, cells were fixed with 70% ethanol, primary and secondary antibody were as

773 described above for immunofluorescence, and DNA was stained with propidium iodide. Cells were

774 analyzed by BD FACSCalibur. The box plot was presented with the bottom line of the box representing

775 the first quartile, the band inside box indicating the median, the top line being the third quartile, the

776 bottom end of whisker denoting data of first quartile minus 1.5 times of interquartile range (no less than

777 0), and the top end of the whisker indicating data of third quartile plus 1.5 times of interquartile. Outliers

778 are not shown. All experiments were performed in duplicate.

779

780 **CRISPRseek analysis of potential off-target sites**

781 Global off-target analyses for DTS3, DTS7, and DTS8 with NmeCas9 sgRNAs were performed using the  
782 Bioconductor package CRISPRseek 1.9.1 [76] with parameter settings tailored for NmeCas9. Specifically,  
783 all parameters are set as default except the following: gRNA.size = 24, PAM = "NNNNNGATT",  
784 PAM.size = 8, RNA.PAM.pattern = "NNNNNGNNN\$", weights = c(0, 0, 0, 0, 0, 0, 0.014, 0, 0, 0.395,  
785 0.317, 0, 0.389, 0.079, 0.445, 0.508, 0.613, 0.851, 0.732, 0.828, 0.615, 0.804, 0.685, 0.583),  
786 max.mismatch = 6, allowed.mismatch.PAM = 7, topN = 10000, min.score = 0. This setting means that  
787 all seven permissive PAM sequences (N<sub>4</sub>GATT, N<sub>4</sub>GCTT, N<sub>4</sub>GT<sub>3</sub>, N<sub>4</sub>GACA, N<sub>4</sub>GACT, N<sub>4</sub>GATA,  
788 N<sub>4</sub>GTCT) were allowed and all off-targets with up to 6 mismatches were collected [the sgRNA length was  
789 changed from 20 to 24; four additional zeros were added to the beginning of the weights series to be  
790 consistent with the gRNA length of 24; and topN (the number of off-target sites displayed) and min.score  
791 (the minimum score of an off-target to be included in the output) were modified to enable identification of  
792 all off-target sites with up to 6 mismatches]. Predicted off-target sites for DTS3, DTS7, and DTS8 with  
793 SpyCas9 sgRNAs were obtained using CRISPRseek 1.9.1 default settings for SpyCas9 (with NGG, NAG,  
794 and NGA PAMs allowed). Batch scripts for high-performance computing running the IBM LSF  
795 scheduling software are included in the supplemental section. Off-target sites were binned according to  
796 the number of mismatches relative to the on-target sequence. The numbers of off-targets for each sgRNA  
797 were counted and plotted as pie charts.

798

799 **GUIDE-seq**

800 We performed GUIDE-seq experiment with some modifications to the original protocol [63], as described  
801 [65]. Briefly, in 24-well format, HEK293T cells were transfected with 150 ng of Cas9, 150 ng of sgRNA,  
802 and 7.5 pmol of annealed GUIDE-seq oligonucleotide using Polyfect transfection reagent (Qiagen) for all  
803 six guides (DTS3, DTS7 and DTS8 for both the NmeCas9 and SpyCas9 systems). Experiments with  
804 DTS7 sgRNAs were repeated using Lipofectamine 3000 transfection reagent (Invitrogen) according to the

805 manufacturer's protocol. 48 h after transfection, genomic DNA was extracted with a DNeasy Blood and  
806 Tissue kit (Qiagen) according to the manufacturer protocol. Library preparation, sequencing, and read  
807 analyses were done according to protocols described previously [63, 65]. Only sites that harbored a  
808 sequence with up to six or ten mismatches with the target site (for SpyCas9 or NmeCas9, respectively)  
809 were considered potential off-target sites. Data were analyzed using the Bioconductor package GUIDEseq  
810 version 1.1.17 (Zhu et al., 2017). For SpyCas9, default setting was used except that min.reads = 2,  
811 max.mismatch = 6, allowed.mismatch.PAM = 2, PAM.pattern = "NNN\$", BSgenomeName = Hsapiens,  
812 txdb = TxDb.Hsapiens.UCSC.hg19.knownGene, orgAnn = org.Hs.egSYMBOL For NmeCas9, default  
813 setting was used except that PAM.size = 8, PAM = "NNNNNGATT", min.reads = 2,  
814 allowed.mismatch.PAM = 4, PAM.pattern = "NNNNNNNN\$", BSgenomeName = Hsapiens, txdb =  
815 TxDb.Hsapiens.UCSC.hg19.knownGene, orgAnn = org.Hs.egSYMBOL. NmeCas9 dataset was  
816 analyzed twice with max.mismatch = 6 and max.mismatch = 10 respectively. The gRNA.size was set to  
817 the length of the gRNA used, and various number of 0's was added at the beginning of weights to make  
818 the length of weights equal to the gRNA size. For example, for gRNA with length 24, weights =  
819 c(0,0,0,0,0, 0, 0.014, 0, 0, 0.395, 0.317, 0, 0.389, 0.079, 0.445, 0.508, 0.613, 0.851, 0.732, 0.828, 0.615,  
820 0.804, 0.685, 0.583) (Zhu et al., 2017). These regions are reported in Supplemental Table 2.

## 821 **SITE-Seq**

822 We performed the SITE-Seq assay as described previously [63]. In 50 mL conical tubes, high molecular  
823 weight genomic DNA (gDNA) was extracted from HEK293T cells using the Blood and Cell Culture DNA  
824 Maxi Kit (Qiagen) according to the manufacturer's protocol. sgRNAs for both NmeCas9 and SpyCas9  
825 RNP assembly were transcribed from PCR-assembled DNA templates containing T7 promoters. Oligo  
826 sequences used in DNA template assembly can found be in Supplemental Table 8. PCR reactions were  
827 performed using Q5 Hot Start High-Fidelity 2X Master Mix (New England Biolabs) with the following  
828 thermal cycling conditions: 98°C for 2 minutes, 30 cycles of 20 seconds at 98°C, 20 seconds at 52°C, 15  
829 seconds at 72°C, and a final extension at 72°C for 2 minutes. sgRNAs were *in vitro* transcribed using the

830 HiScribe T7 High Yield RNA Synthesis Kit (New England Biolabs) according to manufacturer's protocol.  
831 Transcription reactions were digested with 2 units RNase-free DNase I (New England Biolabs) at 37°C  
832 for 10 min; the reaction was stopped by adding EDTA to a final concentration of 35 mM and incubating  
833 at 75°C for 10 min. All guides were purified with RNAClean beads (Beckman Coulter) and quantified  
834 with the Quant-IT Ribogreen RNA Assay kit (ThermoFisher) according to the manufacturers' protocols.  
835 Individual RNPs were prepared by incubating each sgRNA at 95°C for 2 minutes, then allowed to slowly  
836 come to room temperature over 5 minutes. Each sgRNA was then combined with its respective Cas9 in a  
837 3:1 sgRNA:Cas9 molar ratio and incubated at 37°C for 10 minutes in cleavage reaction buffer (20 mM  
838 HEPES, pH 7.4, 150 mM KCl, 10 mM MgCl<sub>2</sub>, 5% glycerol). In 96-well format, 10 µg of gDNA was  
839 treated with 0.2 pmol, 0.8 pmol, 3.2 pmol, and 12.8 pmol of each RNP in 50 µL total volume in cleavage  
840 reaction buffer, in triplicate. Negative control reactions were assembled in parallel and did not include  
841 any RNP. gDNA was treated with RNPs for 4 hours at 37°C. Library preparation and sequencing were  
842 done according to protocols described previously [63] using the Illumina NextSeq platform, and ~3  
843 million reads were obtained for each sample. Any SITE-Seq sites without off-target motifs located within  
844 1 nt of the cut-site were considered false-positives and discarded.

845

#### 846 **Targeted deep sequencing analysis**

847 To measure indel frequencies, targeted deep sequencing analyses were done as previously described [65].  
848 Briefly, we used two-step PCR amplification to produce DNA fragments for each on-target and off-target  
849 site. In the first step, we used locus-specific primers bearing universal overhangs with complementary ends  
850 to the TruSeq adaptor sequences (Supplemental Table 7). DNA was amplified with Phusion High Fidelity  
851 DNA Polymerase (New England Biolabs) using annealing temperatures of 60°C, 64°C or 68°C, depending  
852 on the primer pair. In the second step, the purified PCR products were amplified with a universal forward  
853 primer and an indexed reverse primer to reconstitute the TruSeq adaptors (Supplemental Table 7). Input  
854 DNA was PCR-amplified with Phusion High Fidelity DNA Polymerase (98°C, 15s; 61°C, 25s; 72°C, 18s;  
855 9 cycles) and equal amounts of the products from each treatment group were mixed and run on a 2.5%

856 agarose gel. Full-size products (~250bp in length) were gel-extracted. The purified library was deep  
857 sequenced using a paired-end 150bp MiSeq run.

858 MiSeq data analysis was performed using a suite of Unix-based software tools. First, the quality of  
859 paired-end sequencing reads (R1 and R2 fastq files) was assessed using FastQC  
860 (<http://www.bioinformatics.babraham.ac.uk/projects/fastqc/>). Raw paired-end reads were combined  
861 using paired end read merger (PEAR) [94] to generate single merged high-quality full-length reads. Reads  
862 were then filtered by quality [using Filter FASTQ [95]] to remove those with a mean PHRED quality  
863 score under 30 and a minimum per base score under 24. Each group of reads was then aligned to a  
864 corresponding reference sequence using BWA (version 0.7.5) and SAMtools (version 0.1.19). To  
865 determine indel frequency, size and distribution, all edited reads from each experimental replicate were  
866 combined and aligned, as described above. Indel types and frequencies were then cataloged in a text  
867 output format at each base using bam-readcount (<https://github.com/genome/bam-readcount>). For each  
868 treatment group, the average background indel frequencies (based on indel type, position and frequency)  
869 of the triplicate negative control group were subtracted to obtain the nuclease-dependent indel  
870 frequencies. Indels at each base were marked, summarized and plotted using GraphPad Prism. Deep  
871 sequencing data and the results of statistical tests are reported in Supplemental Table 3.

872 SITE-Seq cell-based validation was performed as previously described with minor modifications  
873 [63]. In brief, SITE-Seq sites were amplified from ~1,000-4,000 template copies per replicate and  
874 sequencing data from Cas9-treated samples were combined to minimize any variability due to uneven  
875 coverage across replicates. Cas9 cleavage sites were registered from the SITE-Seq data, and mutant reads  
876 were defined as any non-reference variant calls within 20 bp of the cut site. Sites with low sequencing  
877 coverage (< 1,000 reads in the combined, Cas9-treated samples or <200 reads in the reference samples)  
878 or >2% variant calls in the reference samples were discarded. Sites were tallied as cellular off-targets if  
879 they accumulated > 0.5% mutant reads in the combined, Cas9-treated samples. This threshold  
880 corresponded to sites that showed unambiguous editing when DNA repair patterns were visually  
881 inspected.

882

883 **List of Abbreviations**

884 **AAV:** adeno-associated virus;  
885 **BLESS:** breaks labelling, enrichment on streptavidin and next-generation sequencing;  
886 **BLISS:** breaks labeling *in situ* and sequencing;  
887 **bp:** base pair;  
888 **Cas:** CRISPR-associated;  
889 **Circle-seq:** circularization for *in vitro* reporting of cleavage effects by sequencing;  
890 **CjeCas9:** *Campylobacter jejuni* Cas9;  
891 **CMV:** cytomegalovirus;  
892 **CRISPR:** clustered, regularly interspaced, short palindromic repeats;  
893 **crRNAs:** CRISPR RNAs;  
894 **dCas9:** “dead” Cas9;  
895 **Digenome-seq:** digested genome sequencing;  
896 **DSB:** double-strand breaks;  
897 **dsODN:** double-stranded oligodeoxynucleotide;  
898 **DTS:** dual target site;  
899 **EF1a:** elongation factor-1a;  
900 **GeoCas9:** *Geobacillus stearothermophilus*;  
901 **GUIDE-seq:** genome-wide unbiased identification of double strand breaks enabled by sequencing;  
902 **HDR:** homology-directed repair;  
903 **HTGTS:** high-throughput genome-wide translocation sequencing;  
904 **IDLV:** integrase-defective lentiviral vector;  
905 **mESC:** mouse embryonic stem cell;  
906 **NHEJ:** non-homologous end joining;  
907 **NLS:** nuclear localization signal;  
908 **NmeCas9:** *Neisseria meningitidis* (strain 8013) Cas9;  
909 **NTS:** NmeCas9 target site;  
910 **PAM:** protospacer adjacent motif;  
911 **RNP:** ribonucleoprotein;  
912 **SauCas9:** *Staphylococcus aureus* Cas9;  
913 **sgRNA:** single-guide RNA;  
914 **SITE-Seq:** selective enrichment and identification of tagged genomic DNA ends by sequencing;  
915 **SpyCas9:** *Streptococcus pyogenes* Cas9;  
916 **T7E1:** T7 Endonuclease 1;  
917 **tracrRNA:** *trans*-acting CRISPR RNA;  
918 **tru-sgRNAs:** truncated sgRNAs.  
919

920 **Declarations**

921 *Ethics approval and consent to participate.* Not applicable.

922 *Consent for publication.* Not applicable.

923 *Availability of data and material.* The deep sequencing data from this study have been submitted to the NCBI

924 Sequence Read Archive (SRA; <http://www.ncbi.nlm.nih.gov/sra>) under accession number XXXXXX.

925 Plasmids will be made available via Addgene.

926 *Competing interests.* E.J.S. is a co-founder and scientific advisor of Intellia Therapeutics. P.D.D, A.H.S,

927 A.M.L, K.M, C.K.F, and P.C are current or former employees of Caribou Biosciences, Inc., a company

928 that develops and commercializes genome engineering technologies; and such individuals may own shares

929 or stock options in Caribou Biosciences.

930 *Funding.* This work was supported by funds from Intellia Therapeutics to E.J.S., and by NIH grant R01

931 GM115911 to E.J.S. and S.A.W.

932 *Authors' contributions.* NA, XDG, PL, AE, AM, RI, AG, KES, and TW carried out genome editing

933 experiments. TW and TGF carried out genotoxicity experiments and analyses. NA, XDG, PL, AM, AG,

934 IJZ, and SAW carried out GUIDE-seq experiments and analysis. PDD, AHS, AML, KM, CKF, and PC

935 carried out SITE-Seq experiments and analyses using NmeCas9 protein supplied by AM. XDG, PL, AM,

936 IJZ, and SAW carried out additional bioinformatic and statistical analyses. All authors analyzed and

937 interpreted data. NA, XDG, PC and EJS wrote the manuscript, and all authors edited the manuscript.

938 *Acknowledgments.* We thank Yin Guo for technical assistance, Wen Xue and members of the Sontheimer

939 and Wolfe laboratories for insightful comments and discussions, and Phil Zamore for the use of his flow

940 cytometer. We are also grateful to the UMMS Deep Sequencing and Molecular Biology Core

941 Laboratories for providing outstanding technical support services for this research project.

942

943 **References**

944 1. Marraffini LA: **CRISPR-Cas immunity in prokaryotes.** *Nature* 2015, **526**:55-61.

945 2. Mohanraju P, Makarova KS, Zetsche B, Zhang F, Koonin EV, van der Oost J: **Diverse**  
946 **evolutionary roots and mechanistic variations of the CRISPR-Cas systems.** *Science* 2016,  
947 **353**:aad5147.

948 3. Sontheimer EJ, Barrangou R: **The bacterial origins of the CRISPR genome-editing**  
949 **revolution.** *Hum Gene Ther* 2015, **26**:413-424.

950 4. Barrangou R, Fremaux C, Deveau H, Richards M, Boyaval P, Moineau S, Romero DA, Horvath  
951 P: **CRISPR provides acquired resistance against viruses in prokaryotes.** *Science* 2007,  
952 **315**:1709-1712.

953 5. Brouns SJ, Jore MM, Lundgren M, Westra ER, Slijkhuis RJ, Snijders AP, Dickman MJ,  
954 Makarova KS, Koonin EV, van der Oost J: **Small CRISPR RNAs guide antiviral defense in**  
955 **prokaryotes.** *Science* 2008, **321**:960-964.

956 6. Marraffini LA, Sontheimer EJ: **CRISPR interference limits horizontal gene transfer in**  
957 **staphylococci by targeting DNA.** *Science* 2008, **322**:1843-1845.

958 7. Makarova KS, Wolf YI, Alkhnbashi OS, Costa F, Shah SA, Saunders SJ, Barrangou R, Brouns  
959 SJ, Charpentier E, Haft DH, et al: **An updated evolutionary classification of CRISPR-Cas**  
960 **systems.** *Nat Rev Microbiol* 2015, **13**:722-736.

961 8. Deltcheva E, Chylinski K, Sharma CM, Gonzales K, Chao Y, Pirzada ZA, Eckert MR, Vogel J,  
962 Charpentier E: **CRISPR RNA maturation by trans-encoded small RNA and host factor**  
963 **RNase III.** *Nature* 2011, **471**:602-607.

964 9. Garneau JE, Dupuis ME, Villion M, Romero DA, Barrangou R, Boyaval P, Fremaux C, Horvath  
965 P, Magadan AH, Moineau S: **The CRISPR/Cas bacterial immune system cleaves**  
966 **bacteriophage and plasmid DNA.** *Nature* 2010, **468**:67-71.

967 10. Sapranauskas R, Gasiunas G, Fremaux C, Barrangou R, Horvath P, Siksnys V: **The**  
968 ***Streptococcus thermophilus* CRISPR/Cas system provides immunity in *Escherichia coli*.**  
969 *Nucleic Acids Res* 2011, **39**:9275-9282.

970 11. Deveau H, Barrangou R, Garneau JE, Labonte J, Fremaux C, Boyaval P, Romero DA, Horvath  
971 P, Moineau S: **Phage response to CRISPR-encoded resistance in *Streptococcus***  
972 ***thermophilus*.** *J Bacteriol* 2008, **190**:1390-1400.

973 12. Mojica FJ, Diez-Villasenor C, Garcia-Martinez J, Almendros C: **Short motif sequences**  
974 **determine the targets of the prokaryotic CRISPR defence system.** *Microbiol* 2009, **155**:733-  
975 740.

976 13. Gasiunas G, Barrangou R, Horvath P, Siksnys V: **Cas9-crRNA ribonucleoprotein complex**  
977 **mediates specific DNA cleavage for adaptive immunity in bacteria.** *Proc Natl Acad Sci USA*  
978 2012, **109**:E2579-2586.

979 14. Jinek M, Chylinski K, Fonfara I, Hauer M, Doudna JA, Charpentier E: **A programmable**  
980 **dual-RNA-guided DNA endonuclease in adaptive bacterial immunity.** *Science* 2012, **337**:816-  
981 821.

982 15. Jiang W, Bikard D, Cox D, Zhang F, Marraffini LA: **RNA-guided editing of bacterial**  
983 **genomes using CRISPR-Cas systems.** *Nat Biotechnol* 2013, **31**:233-239.

984 16. Cho SW, Kim S, Kim JM, Kim JS: **Targeted genome engineering in human cells with**  
985 **the Cas9 RNA-guided endonuclease.** *Nat Biotechnol* 2013, **31**:230-232.

986 17. Cong L, Ran FA, Cox D, Lin S, Barretto R, Habib N, Hsu PD, Wu X, Jiang W, Marraffini LA,  
987 Zhang F: **Multiplex genome engineering using CRISPR/Cas systems.** *Science* 2013, **339**:819-  
988 823.

989 18. Hwang WY, Fu Y, Reyon D, Maeder ML, Tsai SQ, Sander JD, Peterson RT, Yeh JR, Joung JK:  
990 **Efficient genome editing in zebrafish using a CRISPR-Cas system.** *Nat Biotechnol* 2013, **31**:227-  
991 229.

992 19. Jinek M, East A, Cheng A, Lin S, Ma E, Doudna J: **RNA-programmed genome editing in**  
993 **human cells.** *eLife* 2013, **2**:e00471.

994 20. Mali P, Yang L, Esvelt KM, Aach J, Guell M, DiCarlo JE, Norville JE, Church GM: **RNA-**  
995 **guided human genome engineering via Cas9.** *Science* 2013, **339**:823-826.

996 21. Urnov FD: **Genome Editing B.C. (Before CRISPR): Lasting Lessons from the “Old**  
997 **Testament”.** *CRISPR J* 2018, **1**:34-46.

998 22. Hsu PD, Lander ES, Zhang F: **Development and applications of CRISPR-Cas9 for**  
999 **genome engineering.** *Cell* 2014, **157**:1262-1278.

1000 23. Komor AC, Badran AH, Liu DR: **CRISPR-Based Technologies for the Manipulation of**  
1001 **Eukaryotic Genomes.** *Cell* 2017, **168**:20-36.

1002 24. Sternberg SH, Doudna JA: **Expanding the Biologist's Toolkit with CRISPR-Cas9.** *Mol*  
1003 *Cell* 2015, **58**:568-574.

1004 25. Dominguez AA, Lim WA, Qi LS: **Beyond editing: repurposing CRISPR-Cas9 for**  
1005 **precision genome regulation and interrogation.** *Nat Rev Mol Cell Biol* 2016, **17**:5-15.

1006 26. Wang H, La Russa M, Qi LS: **CRISPR/Cas9 in Genome Editing and Beyond.** *Annu Rev*  
1007 *Biochem* 2016, **85**:227-264.

1008 27. Zetsche B, Gootenberg JS, Abudayyeh OO, Slaymaker IM, Makarova KS, Essletzbichler P, Volz  
1009 SE, Joung J, van der Oost J, Regev A, et al: **Cpf1 is a single RNA-guided endonuclease of a class**  
1010 **2 CRISPR-Cas system.** *Cell* 2015, **163**:759-771.

1011 28. Shmakov S, Smargon A, Scott D, Cox D, Pyzocha N, Yan W, Abudayyeh OO, Gootenberg JS,  
1012 Makarova KS, Wolf YI, et al: **Diversity and evolution of class 2 CRISPR-Cas systems.** *Nat Rev*  
1013 *Microbiol* 2017, **15**:169-182.

1014 29. Fu Y, Foden JA, Khayter C, Maeder ML, Reyon D, Joung JK, Sander JD: **High-frequency**  
1015 **off-target mutagenesis induced by CRISPR-Cas nucleases in human cells.** *Nat Biotechnol* 2013,  
1016 **31**:822-826.

1017 30. Hsu PD, Scott DA, Weinstein JA, Ran FA, Konermann S, Agarwala V, Li Y, Fine EJ, Wu X,  
1018 Shalem O, et al: **DNA targeting specificity of RNA-guided Cas9 nucleases.** *Nat Biotechnol* 2013,  
1019 **31**:827-832.

1020 31. Bolukbasi MF, Gupta A, Wolfe SA: **Creating and evaluating accurate CRISPR-Cas9**  
1021 **scalpels for genomic surgery.** *Nat Methods* 2015, **13**:41-50.

1022 32. Casini A, Olivieri M, Petris G, Montagna C, Reginato G, Maule G, Lorenzin F, Prandi D,  
1023 Romanel A, Demichelis F, et al: **A highly specific SpCas9 variant is identified by *in vivo***  
1024 **screening in yeast.** *Nat Biotechnol* 2018, **36**:265-271.

1025 33. Chen JS, Dagdas YS, Kleinstiver BP, Welch MM, Sousa AA, Harrington LB, Sternberg SH,  
1026 Joung JK, Yildiz A, Doudna JA: **Enhanced proofreading governs CRISPR-Cas9 targeting**  
1027 **accuracy.** *Nature* 2017.

1028 34. Tsai SQ, Joung JK: **Defining and improving the genome-wide specificities of CRISPR-**  
1029 **Cas9 nucleases.** *Nat Rev Genet* 2016, **17**:300-312.

1030 35. Tycko J, Myer VE, Hsu PD: **Methods for optimizing CRISPR-Cas9 genome editing**  
1031 **specificity.** *Mol Cell* 2016, **63**:355-370.

1032 36. Yin H, Song CQ, Suresh S, Kwan SY, Wu Q, Walsh S, Ding J, Bogorad RL, Zhu LJ, Wolfe SA,  
1033 et al: **Partial DNA-guided Cas9 enables genome editing with reduced off-target activity.** *Nat*  
1034 *Chem Biol* 2018, **14**:311-316.

1035 37. Kleinstiver BP, Pattanayak V, Prew MS, Tsai SQ, Nguyen NT, Zheng Z, Joung JK: **High-**  
1036 **fidelity CRISPR-Cas9 nucleases with no detectable genome-wide off-target effects.** *Nature*  
1037 2016, **529**:490-495.

1038 38. Slaymaker IM, Gao L, Zetsche B, Scott DA, Yan WX, Zhang F: **Rationally engineered Cas9**  
1039 **nucleases with improved specificity.** *Science* 2016, **351**:84-88.

1040 39. Jiang F, Taylor DW, Chen JS, Kornfeld JE, Zhou K, Thompson AJ, Nogales E, Doudna JA:  
1041 **Structures of a CRISPR-Cas9 R-loop complex primed for DNA cleavage.** *Science* 2016,  
1042 **351**:867-871.

1043 40. Jiang F, Zhou K, Ma L, Gressel S, Doudna JA: **A Cas9-guide RNA complex preorganized**  
1044 **for target DNA recognition.** *Science* 2015, **348**:1477-1481.

1045 41. Jinek M, Jiang F, Taylor DW, Sternberg SH, Kaya E, Ma E, Anders C, Hauer M, Zhou K, Lin  
1046 S, et al: **Structures of Cas9 endonucleases reveal RNA-mediated conformational activation.**  
1047 *Science* 2014, **343**:1247997.

1048 42. Nishimasu H, Ran FA, Hsu PD, Konermann S, Shehata SI, Dohmae N, Ishitani R, Zhang F,  
1049 Nureki O: **Crystal structure of Cas9 in complex with guide RNA and target DNA.** *Cell* 2014,  
1050 **156**:935-949.

1051 43. Chylinski K, Makarova KS, Charpentier E, Koonin EV: **Classification and evolution of**  
1052 **type II CRISPR-Cas systems.** *Nucleic Acids Res* 2014, **42**:6091-6105.

1053 44. Fonfara I, Le Rhun A, Chylinski K, Makarova KS, Lecrivain AL, Bzdrenga J, Koonin EV,  
1054 Charpentier E: **Phylogeny of Cas9 determines functional exchangeability of dual-RNA and**  
1055 **Cas9 among orthologous type II CRISPR-Cas systems.** *Nucleic Acids Res* 2014, **42**:2577-2590.

1056 45. Briner AE, Donohoue PD, Gomaa AA, Selle K, Slorach EM, Nye CH, Haurwitz RE, Beisel CL,  
1057 May AP, Barrangou R: **Guide RNA functional modules direct Cas9 activity and**  
1058 **orthogonality.** *Mol Cell* 2014, **56**:333-339.

1059 46. Esvelt KM, Mali P, Braff JL, Moosburner M, Yaung SJ, Church GM: **Orthogonal Cas9**  
1060 **proteins for RNA-guided gene regulation and editing.** *Nat Methods* 2013, **10**:1116-1121.

1061 47. Kim E, Koo T, Park SW, Kim D, Kim K, Cho HY, Song DW, Lee KJ, Jung MH, Kim S, et al:  
1062 **In vivo genome editing with a small Cas9 orthologue derived from *Campylobacter jejuni*.**  
1063 *Nat Commun* 2017, **8**:14500.

1064 48. Ran FA, Cong L, Yan WX, Scott DA, Gootenberg JS, Kriz AJ, Zetsche B, Shalem O, Wu X,  
1065 Makarova KS, et al: **In vivo genome editing using *Staphylococcus aureus* Cas9.** *Nature* 2015,  
1066 **520**:186-191.

1067 49. Mir A, Edraki A, Lee J, Sontheimer EJ: **Type II-C CRISPR-Cas9 biology, mechanism and**  
1068 **application.** *ACS Chemical Biology* 2018:in press.

1069 50. Zhang Y: **The CRISPR-Cas9 system in *Neisseria* spp.** *Pathog Dis* 2017, **75**.

1070 51. Zhang Y, Heidrich N, Ampattu BJ, Gunderson CW, Seifert HS, Schoen C, Vogel J, Sontheimer  
1071 EJ: **Processing-independent CRISPR RNAs limit natural transformation in *Neisseria***  
1072 **meningitidis.** *Mol Cell* 2013, **50**:488-503.

1073 52. Zhang Y, Rajan R, Seifert HS, Mondragón A, Sontheimer EJ: **DNase H activity of *Neisseria***

1074 ***meningitidis Cas9***. *Mol Cell* 2015, **60**:242-255.

1075 53. Hou Z, Zhang Y, Propson NE, Howden SE, Chu LF, Sontheimer EJ, Thomson JA: **Efficient**

1076 **genome engineering in human pluripotent stem cells using Cas9 from *Neisseria***

1077 ***meningitidis***. *Proc Natl Acad Sci USA* 2013, **110**:15644-15649.

1078 54. Lee CM, Cradick TJ, Bao G: **The *Neisseria meningitidis* CRISPR-Cas9 system enables**

1079 **specific genome editing in mammalian cells**. *Mol Ther* 2016, **24**:645-654.

1080 55. Ma E, Harrington LB, O'Connell MR, Zhou K, Doudna JA: **Single-Stranded DNA Cleavage**

1081 **by Divergent CRISPR-Cas9 Enzymes**. *Mol Cell* 2015, **60**:398-407.

1082 56. Rousseau BA, Hou Z, Gramelspacher MJ, Zhang Y: **Programmable RNA cleavage and**

1083 **recognition by a natural CRISPR-Cas9 system from *Neisseria meningitidis***. *Molecular Cell*

1084 2018:in press.

1085 57. Harrington LB, Doxzen KW, Ma E, Liu JJ, Knott GJ, Edraki A, Garcia B, Amrani N, Chen JS,

1086 Cofsky JC, et al: **A Broad-Spectrum Inhibitor of CRISPR-Cas9**. *Cell* 2017, **170**:1224-1233 e1215.

1087 58. Pawluk A, Amrani N, Zhang Y, Garcia B, Hidalgo-Reyes Y, Lee J, Edraki A, Shah M,

1088 Sontheimer EJ, Maxwell KL, Davidson AR: **Naturally occurring off-switches for CRISPR-Cas9**.

1089 *Cell* 2016.

1090 59. Sontheimer EJ, Davidson AR: **Inhibition of CRISPR-Cas systems by mobile genetic**

1091 **elements**. *Curr Opin Microbiol* 2017, **37**:120-127.

1092 60. Rauch BJ, Silvis MR, Hultquist JF, Waters CS, McGregor MJ, Krogan NJ, Bondy-Denomy J:

1093 **Inhibition of CRISPR-Cas9 with Bacteriophage Proteins**. *Cell* 2017, **168**:150-158 e110.

1094 61. Hynes AP, Rousseau GM, Lemay M-L, Horvath P, Romero DA, Fremaux C, Moineau S: **An**  
1095 **anti-CRISPR from a virulent streptococcal phage inhibits *Streptococcus pyogenes* Cas9.**  
1096 *Nature Microbiology* 2017, **2**:1374-1380.

1097 62. Kearns NA, Pham H, Tabak B, Genga RM, Silverstein NJ, Garber M, Maehr R: **Functional**  
1098 **annotation of native enhancers with a Cas9-histone demethylase fusion.** *Nat Methods* 2015,  
1099 **12**:401-403.

1100 63. Tsai SQ, Zheng Z, Nguyen NT, Liebers M, Topkar VV, Thapar V, Wyveldens N, Khayter C,  
1101 Iafrate AJ, Le LP, et al: **GUIDE-seq enables genome-wide profiling of off-target cleavage by**  
1102 **CRISPR-Cas nucleases.** *Nat Biotechnol* 2014, **33**:187-197.

1103 64. Cameron P, Fuller CK, Donohoue PD, Jones BN, Thompson MS, Carter MM, Gradia S, Vidal  
1104 B, Garner E, Slorach EM, et al: **Mapping the genomic landscape of CRISPR-Cas9 cleavage.** *Nat*  
1105 *Methods* 2017, **14**:600-606.

1106 65. Bolukbasi MF, Gupta A, Oikemus S, Derr AG, Garber M, Brodsky MH, Zhu LJ, Wolfe SA:  
1107 **DNA-binding-domain fusions enhance the targeting range and precision of Cas9.** *Nat*  
1108 *Methods* 2015, **12**:1150-1156.

1109 66. Wilson KA, McEwen AE, Pruett-Miller SM, Zhang J, Kildebeck EJ, Porteus MH: **Expanding**  
1110 **the Repertoire of Target Sites for Zinc Finger Nuclease-mediated Genome Modification.**  
1111 *Mol Ther Nucleic Acids* 2013, **2**:e88.

1112 67. Guan C, Kumar S, Kucera R, Ewel A: **Changing the enzymatic activity of T7**  
1113 **endonuclease by mutations at the beta-bridge site: alteration of substrate specificity**  
1114 **profile and metal ion requirements by mutation distant from the catalytic domain.**  
1115 *Biochemistry* 2004, **43**:4313-4322.

1116 68. Cho SW, Kim S, Kim Y, Kweon J, Kim HS, Bae S, Kim JS: **Analysis of off-target effects of**  
1117 **CRISPR/Cas-derived RNA-guided endonucleases and nickases.** *Genome Res* 2014, **24**:132-141.

1118 69. Fu Y, Sander JD, Reyon D, Cascio VM, Joung JK: **Improving CRISPR-Cas nuclease**  
1119 **specificity using truncated guide RNAs.** *Nat Biotechnol* 2014, **32**:279-284.

1120 70. Hwang WY, Fu Y, Reyon D, Maeder ML, Kaini P, Sander JD, Joung JK, Peterson RT, Yeh JR:  
1121 **Heritable and precise zebrafish genome editing using a CRISPR-Cas system.** *PLoS One*  
1122 2013, **8**:e68708.

1123 71. Ran FA, Hsu PD, Lin CY, Gootenberg JS, Konermann S, Trevino AE, Scott DA, Inoue A,  
1124 Matoba S, Zhang Y, Zhang F: **Double nicking by RNA-guided CRISPR Cas9 for enhanced**  
1125 **genome editing specificity.** *Cell* 2013, **154**:1380-1389.

1126 72. Santos-Pereira JM, Aguilera A: **R loops: new modulators of genome dynamics and**  
1127 **function.** *Nature Reviews Genetics* 2015, **16**:583-597.

1128 73. Ciccia A, Elledge SJ: **The DNA damage response: making it safe to play with knives.**  
1129 *Molecular Cell* 2010, **40**:179-204.

1130 74. Chen PB, Chen HV, Acharya D, Rando OJ, Fazzio TG: **R loops regulate promoter-**  
1131 **proximal chromatin architecture and cellular differentiation.** *Nature Structural & Molecular*  
1132 *Biology* 2015, **22**:999-1007.

1133 75. Aoudia M, Eid A, Ali Z, Cradick T, Lee C, Deshmukh H, Atef A, AbuSamra D, Gadhoun SZ,  
1134 Merzaban J, et al: **Efficient fdCas9 Synthetic Endonuclease with Improved Specificity for**  
1135 **Precise Genome Engineering.** *PLoS One* 2015, **10**:e0133373.

1136 76. Zhu LJ, Holmes BR, Aronin N, Brodsky MH: **CRISPRseek: a bioconductor package to**  
1137 **identify target-specific guide RNAs for CRISPR-Cas9 genome-editing systems.** *PLoS One*  
1138 2014, **9**:e108424.

1139 77. Tsai SQ, Nguyen NT, Malagon-Lopez J, Topkar VV, Aryee MJ, Joung JK: **CIRCLE-seq: a**  
1140 **highly sensitive in vitro screen for genome-wide CRISPR-Cas9 nuclease off-targets.** *Nat*  
1141 *Methods* 2017, **14**:607-614.

1142 78. Yan WX, Mirzazadeh R, Garnerone S, Scott D, Schneider MW, Kallas T, Custodio J,  
1143 Wernersson E, Li Y, Gao L, et al: **BLISS is a versatile and quantitative method for genome-**  
1144 **wide profiling of DNA double-strand breaks.** *Nat Commun* 2017, **8**:15058.

1145 79. Zhu LJ, Lawrence M, Gupta A, Pagés H, Kucukural A, Garber M, Wolfe SA: **GUIDEseq: a**  
1146 **bioconductor package to analyze GUIDE-Seq datasets for CRISPR-Cas nucleases.** *BMC*  
1147 *Genomics* 2017, **18**:379.

1148 80. Chen F, Ding X, Feng Y, Seebeck T, Jiang Y, Davis GD: **Targeted activation of diverse**  
1149 **CRISPR-Cas systems for mammalian genome editing via proximal CRISPR targeting.** *Nat*  
1150 *Commun* 2017, **8**:14958.

1151 81. Dong, Guo M, Wang S, Zhu Y, Wang S, Xiong Z, Yang J, Xu Z, Huang Z: **Structural basis**  
1152 **of CRISPR-SpyCas9 inhibition by an anti-CRISPR protein.** *Nature* 2017, **546**:436-439.

1153 82. Shin CS, Jiang F, Liu J-J, Bray NL, Rauch BJ, Baik SH, Nogales E, Bondy-Denomy J, Corn JE,  
1154 Doudna JA: **Disabling Cas9 by an anti-CRISPR DNA mimic.** *Science Advances* 2017:, in press.

1155 83. Yang H, Patel DJ: **Inhibition Mechanism of an Anti-CRISPR Suppressor AcrIIA4**  
1156 **Targeting SpyCas9.** *Mol Cell* 2017.

1157 84. Fu BX, Hansen LL, Artiles KL, Nonet ML, Fire AZ: **Landscape of target:guide homology**  
1158 **effects on Cas9-mediated cleavage.** *Nucleic Acids Res* 2014, **42**:13778-13787.

1159 85. Pattanayak V, Lin S, Guilinger JP, Ma E, Doudna JA, Liu DR: **High-throughput profiling of**  
1160 **off-target DNA cleavage reveals RNA-programmed Cas9 nuclease specificity.** *Nat Biotechnol*  
1161 2013, **31**:839-843.

1162 86. Kim S, Kim D, Cho SW, Kim J, Kim JS: **Highly efficient RNA-guided genome editing in**  
1163 **human cells via delivery of purified Cas9 ribonucleoproteins.** *Genome Res* 2014, **24**:1012-1019.

1164 87. Zuris JA, Thompson DB, Shu Y, Guilinger JP, Bessen JL, Hu JH, Maeder ML, Joung JK, Chen  
1165 Z-Y, Liu DR: **Cationic lipid-mediated delivery of proteins enables efficient protein-based**  
1166 **genome editing *in vitro* and *in vivo*.** *Nat Biotechnol* 2015, **33**:73-80.

1167 88. Bisaria N, Jarmoskaite I, Herschlag D: **Lessons from Enzyme Kinetics Reveal Specificity**  
1168 **Principles for RNA-Guided Nucleases in RNA Interference and CRISPR-Based Genome**  
1169 **Editing.** *Cell Syst* 2017, **4**:21-29.

1170 89. Villefranc JA, Amigo J, Lawson ND: **Gateway compatible vectors for analysis of gene**  
1171 **function in the zebrafish.** *Dev Dyn* 2007, **236**:3077-3087.

1172 90. Kearns NA, Pham H, Tabak B, Genga RM, Silverstein NJ, Garber M, Maehr R: **Functional**  
1173 **annotation of native enhancers with a Cas9-histone demethylase fusion.** *Nat Methods* 2015,  
1174 **12**:401-403.

1175 91. Mou H, Smith JL, Peng L, Yin H, Moore J, Zhang XO, Song CQ, Sheel A, Wu Q, Ozata DM,  
1176 et al: **CRISPR/Cas9-mediated genome editing induces exon skipping by alternative**  
1177 **splicing or exon deletion.** *Genome Biol* 2017, **18**:108.

1178 92. Gupta A, Hall VL, Kok FO, Shin M, McNulty JC, Lawson ND, Wolfe SA: **Targeted**  
1179 **chromosomal deletions and inversions in zebrafish.** *Genome Res* 2013, **23**:1008-1017.

1180 93. Guschin DY, Waite AJ, Katibah GE, Miller JC, Holmes MC, Rebar EJ: **A rapid and general**  
1181 **assay for monitoring endogenous gene modification.** *Methods Mol Biol* 2010, **649**:247-256.

1182 94. Zhang J, Kober K, Flouri T, Stamatakis A: **PEAR: a fast and accurate Illumina Paired-**  
1183 **End reAd mergeR.** *Bioinformatics* 2014, **30**:614-620.

1184 95. Blankenberg D, Gordon A, Von Kuster G, Coraor N, Taylor J, Nekrutenko A, Galaxy T:  
1185 **Manipulation of FASTQ data with Galaxy.** *Bioinformatics* 2010, **26**:1783-1785.

1186

1187

1188 **Figures**

1189

1190 **Figure 1.** NmeCas9 expression and activity in human (HEK293T) cells. (A) Western blot detection of HA-tagged  
1191 NmeCas9 in transiently transfected HEK293T cells. Lane 1: Cells transfected with SpyCas9 plasmid under the  
1192 control of the CMV promoter. Lane 2: Cells transfected with NmeCas9 plasmid under the control of the elongation  
1193 factor-1α (EF1α) promoter. Lane 3: Cells expressing NmeCas9 and a non-targeting sgRNA (nt-sgRNA), which lacks  
1194 a complementary site in the human genome. Lane 4: Cells expressing NmeCas9 and a sgRNA targeting  
1195 chromosomal site NTS3. Upper panel: Anti-HA western blot. Lower panel: Anti-GAPDH western blot as a loading  
1196 control. (B) NmeCas9 targeting co-transfected split-GFP reporter with ps9, ps24 and ps25 sites. Plasmid cleavage by  
1197 SpyCas9 is used as a positive control, and a reporter without a guide-complementary site (No ps: no protospacer) is  
1198 used as a negative control to define background levels of recombination leading to GFP+ cells. (C) NmeCas9  
1199 programmed independently with different sgRNAs targeting eleven genomic sites flanked by an N<sub>4</sub>GATT PAM,  
1200 detected by T7E1 analysis. (D) Quantitation of editing efficiencies from three independent biological replicates  
1201 performed on different days. Error bars indicate ± standard error of the mean (± s.e.m.). (E) Genomic lesions with  
1202 NmeCas9 programmed independently with different guides in different cell lines and using different methods of  
1203 delivery.

1204

1205 **Figure 2.** NmeCas9 guide length requirements in mammalian cells. (A) Split-GFP activity profile of NmeCas9  
1206 cleavage with ps9 sgRNAs bearing spacers of varying lengths (18-24 nts) along with 5'-terminal G residues to enable  
1207 transcription. Bars represent mean values  $\pm$  s.e.m. from three independent biological replicates performed on  
1208 different days. (B) T7EI analysis of editing efficiencies at the NTS33 genomic target site (with an N<sub>4</sub>GATT PAM)  
1209 with sgRNAs bearing spacers of varying lengths (13-25 nts) with 1-2 5'-terminal G residues. (C) Quantitation of  
1210 lesion efficiencies (of experiment in B) from three independent biological replicates performed on different days.  
1211 Error bars indicate  $\pm$  standard error of the mean ( $\pm$  s.e.m.). (D) As in (B), but targeting the NTS32 genomic site (with  
1212 an N<sub>4</sub>GCTT PAM). (E) Quantitation of lesion efficiencies (of experiment in D) from three independent biological  
1213 replicates performed on different days. Error bars indicate  $\pm$  standard error of the mean ( $\pm$  s.e.m.).

1214

1215 **Figure 3.** Characterization of functional PAM sequences in human (HEK293T) cells. (A) Split-GFP activity profile  
1216 of NmeCas9 cleavage with ps9 sgRNA, with the target site flanked by different PAM sequences. Bars represent  
1217 mean values  $\pm$  s.e.m. from three independent biological replicates performed on different days. (B) T7E1 analysis of  
1218 editing efficiencies at seven genomic sites flanked by PAM variants, as indicated. Products resulting from NmeCas9  
1219 genome editing are denoted by the red dots. (C) Quantitation of data from (B), as well as an additional site (NTS31;  
1220 N<sub>4</sub>GACA PAM) that was not successfully edited. Bars represent mean values  $\pm$  s.e.m. from three independent  
1221 biological replicates performed on different days.

1222

1223 **Figure 4.** NmeCas9 and SpyCas9 have comparable editing efficiencies in human (HEK293T) cells when targeting  
1224 the same chromosomal sites. (A) Western blot analysis of NmeCas9 and SpyCas9. HEK293T cells were transfected  
1225 with the indicated Cas9 ortholog cloned in the same plasmid backbone, and fused to the same HA epitope tags and  
1226 NLSSs. Top panel: anti-HA western blot (EP, empty sgRNA plasmid). Bottom panel: anti-GAPDH western blot, used  
1227 as a loading control. Mobilities of protein markers are indicated. (B) T7E1 analysis of three previously validated  
1228 SpyCas9 guides targeting the *A4VS1* locus, in comparison with NmeCas9 guides targeting nearby *A4VS1* sites (mean  
1229  $\pm$  s.e.m.,  $n = 3$ ). (C) Representative T7EI analyses comparing editing efficiencies at the dual target sites DTS1,  
1230 DTS3, DTS7, DTS8, and NTS7, using the indicated Cas9/sgRNA combinations. (D) Quantitation of data from (C)  
1231 (mean  $\pm$  s.e.m.,  $n = 3$ ).

1232

1233 **Figure 5.** Bioinformatic and empirical comparison of NmeCas9 and SpyCas9 off-target sites within the human  
1234 genome. (A) Genome-wide computational (CRISPRseek) predictions of off-target sites for NmeCas9 (with N<sub>4</sub>GN<sub>3</sub>  
1235 PAMs) and SpyCas9 (with NGG, NGA, and NAG PAMs) with DTS3, DTS7 and DTS8 sgRNAs. Predicted off-  
1236 target sites were binned based on the number of mismatches (up to six) with the guide sequences. (B) GUIDE-Seq  
1237 analysis of off-target sites in HEK293T cells with sgRNAs targeting DTS3, DTS7 and DTS8, using either SpyCas9  
1238 or NmeCas9, and with up to 6 mismatches to the sgRNAs. The numbers of detected off-target sites are indicated at  
1239 the top of each bar. (C) Numbers of independent GUIDE-Seq reads for the on- and off-target sites for all six  
1240 Cas9/sgRNA combinations from (B) (SpyCas9, red; NmeCas9, green), binned by the number of mismatches with  
1241 the corresponding guide. (D) Targeted deep sequencing analysis of lesion efficiencies at on- and off-target sites from  
1242 (A) or (B) with SpyCas9 (left, red) or NmeCas9 (right, green). Data for off-target sites are in grey. For SpyCas9, all  
1243 off-target sites were chosen from (B) based on the highest GUIDE-Seq read counts for each guide (Supplemental  
1244 Table 3). For NmeCas9, in addition to those candidate off-target sites obtained from GUIDE-Seq (C), we also  
1245 assayed one or two potential off-target sites (designated with the “-CS” suffix) predicted by CRISPRseek as the  
1246 closest near-cognate matches with permissive PAMs. Data are mean values  $\pm$  s.e.m. from three biological replicates  
1247 performed on different days.

1248

1249 **Figure 6.** Off-target analyses for additional NmeCas9 sgRNAs, targeting sites with consensus and variant PAMs. (A)  
1250 Number of GUIDE-Seq reads for the on-target sites, with the PAM sequences for each site indicated underneath. (B)  
1251 Number of GUIDE-Seq-detected off-target sites using the Bioconductor package GUIDEseq version 1.1.17 [79]  
1252 with default settings except that PAM.size = 8, PAM = "NNNNNGATT", min.reads = 2, max.mismatch = 6,  
1253 allowed.mismatch.PAM = 4, PAM.pattern = "NNNNNNNN\$", BSgenomeName = Hsapiens, txdb =  
1254 TxDb.Hsapiens.UCSC.hg19.knownGene, orgAnn = org.Hs.egSYMBOL gRNA.size was set to length of the gRNA  
1255 used, and various number of 0's were added at the beginning of weights to make the length of weights equal to the  
1256 gRNA size. For example, for gRNA with length 24, weights = c(0,0,0,0, 0, 0.014, 0, 0, 0.395, 0.317, 0, 0.389,  
1257 0.079, 0.445, 0.508, 0.613, 0.851, 0.732, 0.828, 0.615, 0.804, 0.685, 0.583) for all sixteen sgRNAs used in (A). (C)  
1258 Lesion efficiencies for the on-target sites as measured by PCR and high-throughput sequencing. Data are mean  
1259 values  $\pm$  s.e.m. from three biological replicates performed on different days. (D) NmeCas9 lesion efficiencies at the

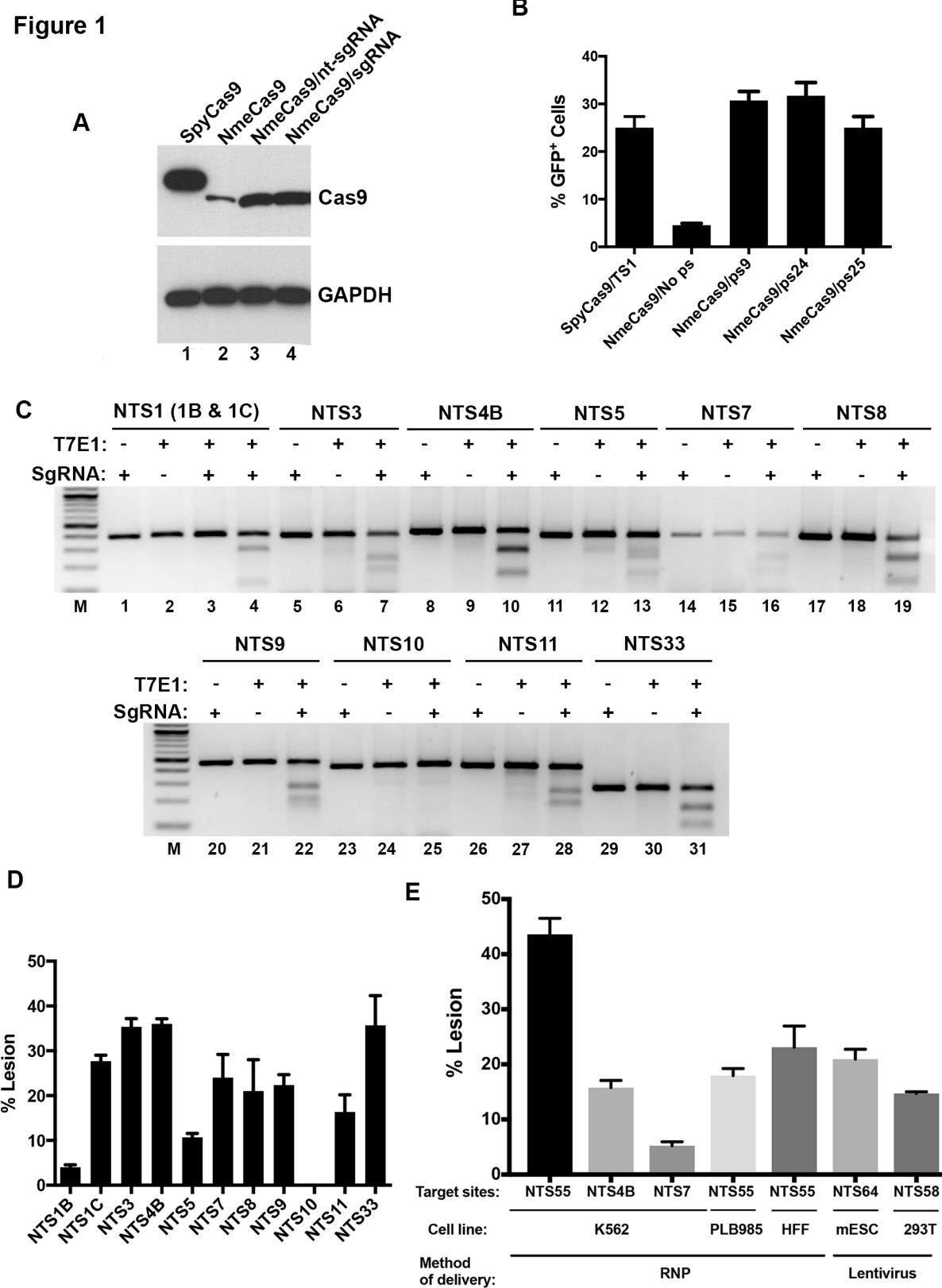
1260 NTS1C (left) and NTS25 (right) on-target sites, and at the off-target sites detected by GUIDE-Seq from (B), as  
1261 measured by PCR and high-throughput sequencing. Data are mean values  $\pm$  s.e.m. from three biological replicates  
1262 performed on different days. (E) Schematic diagrams of NmeCas9 sgRNA/DNA R-loops for the NTS1C (left) and  
1263 NTS25 (right) sgRNAs, at the GUIDE-Seq-detected on- and off-target sites. Black, DNA residues; boxed nts, PAM;  
1264 red line, NmeCas9 cleavage site; cyan and purple, mismatch/wobble and complementary nts (respectively) in the  
1265 NmeCas9 sgRNA guide region; green, NmeCas9 sgRNA repeat nts. (F) Comparison of NmeCas9 and SpyCas9  
1266 biochemical off-target sites using SITE-Seq analysis.

1267

1268 **Figure 7.** Guide truncation can suppress off-target editing by NmeCas9. (A) Lesion efficiencies at the NTS1C (on-  
1269 target, red) and NTS1C-OT1 (off-target, orange) genomic sites, after editing by NmeCas9 and NTS1C sgRNAs of  
1270 varying lengths, as measured by PCR and high-throughput sequencing. Data are mean values  $\pm$  s.e.m. from three  
1271 biological replicates performed on different days. (B) As in (A), but using sgRNAs perfectly complementary to the  
1272 NTS1C-OT1 genomic site.

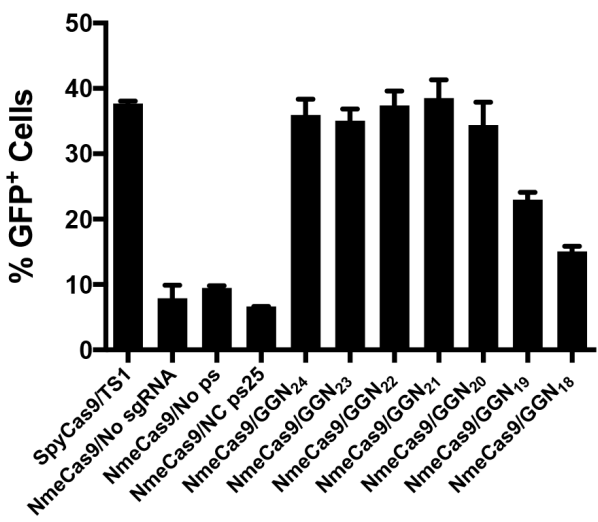
1273

Figure 1

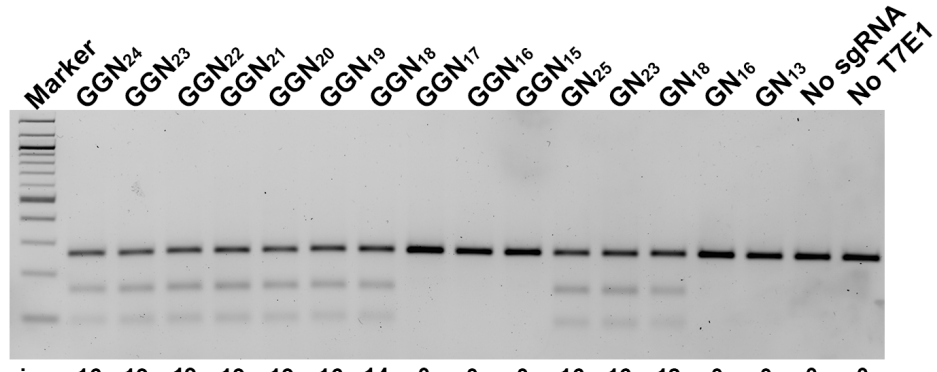


## Figure 2

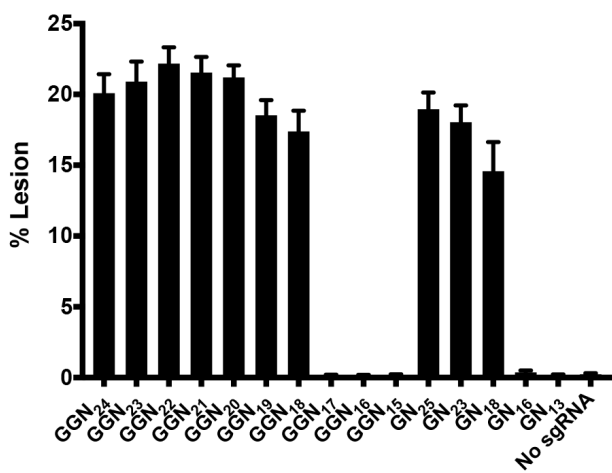
A



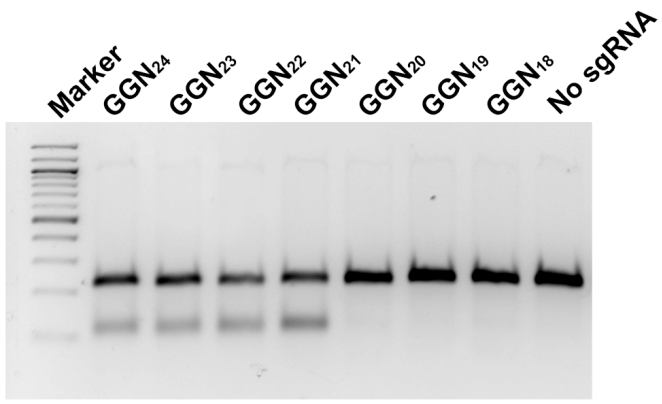
B



C



D



E

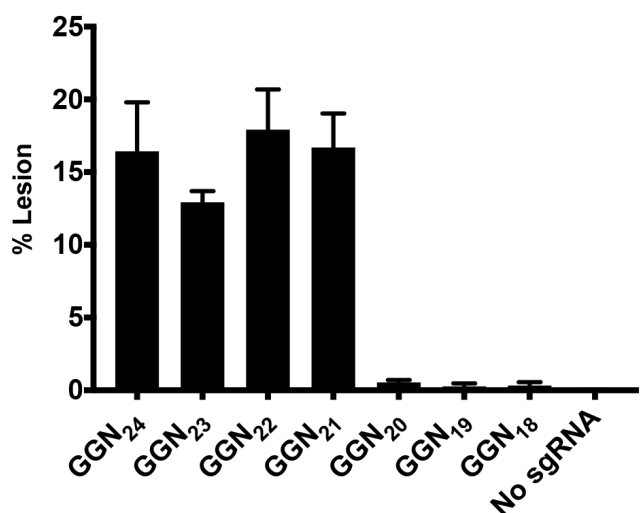
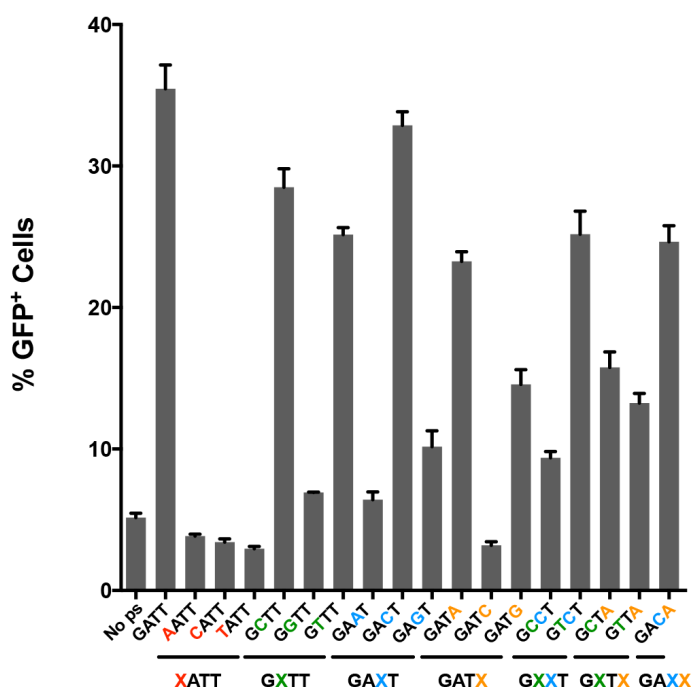
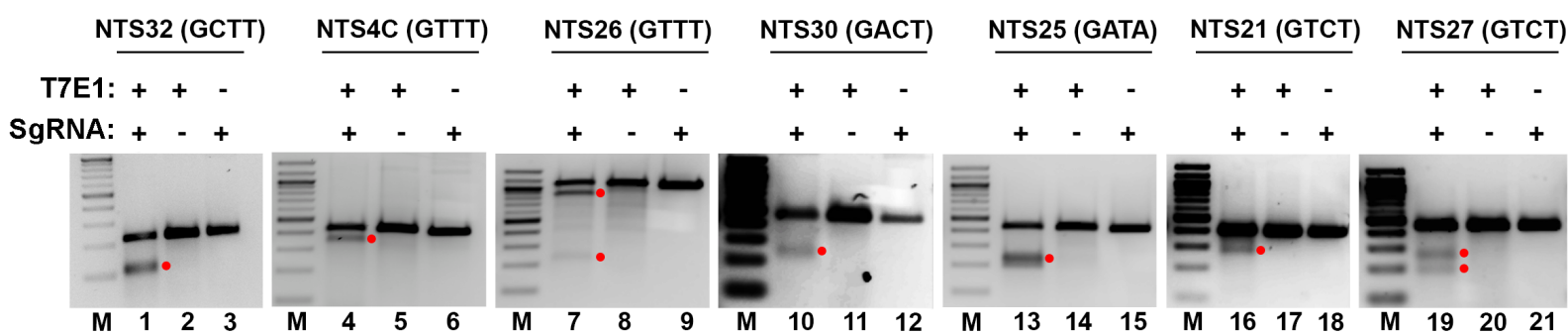


**Figure 3**

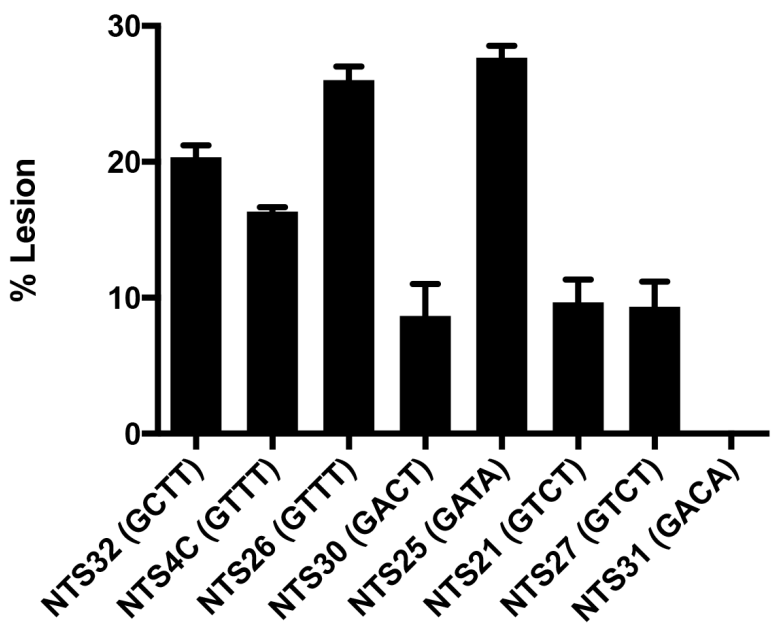
**A**

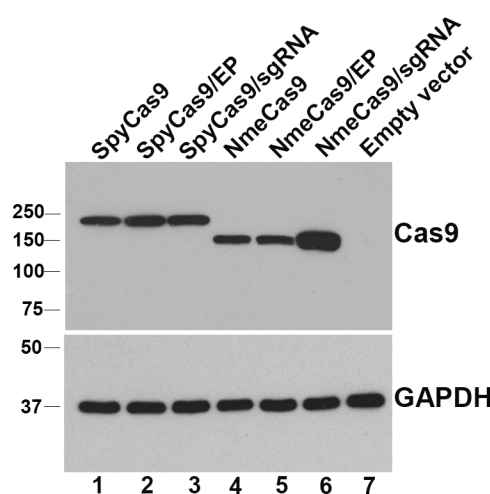
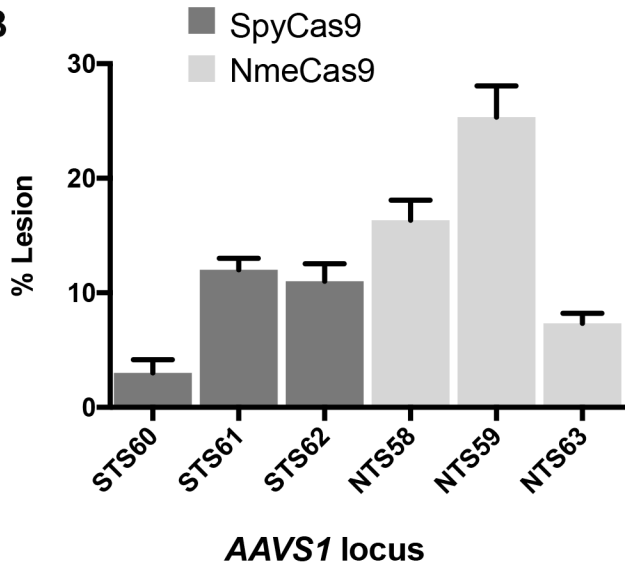
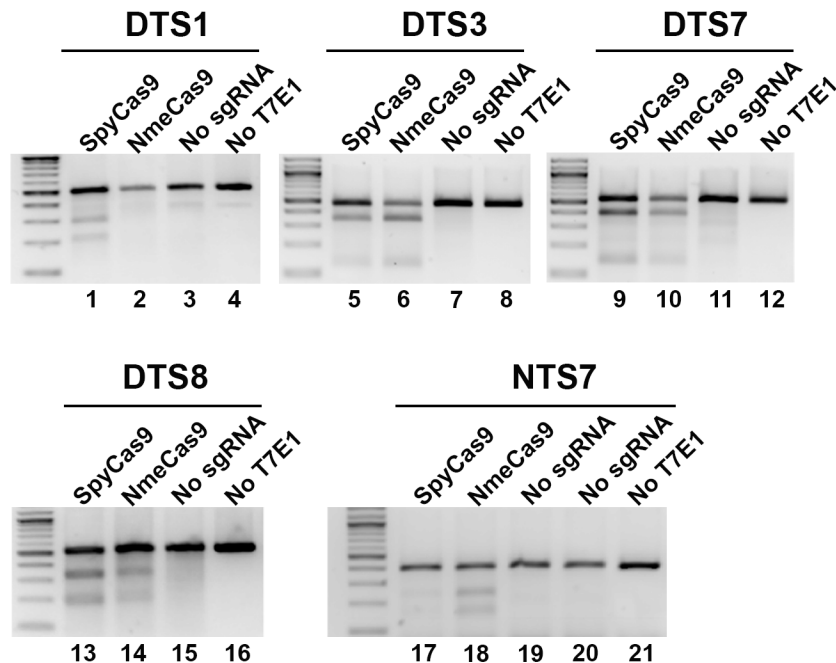
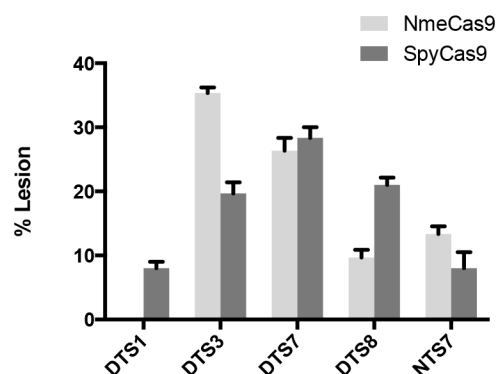


**B**



**C**



**Figure 4****A****B****C****D**

**Figure 5**

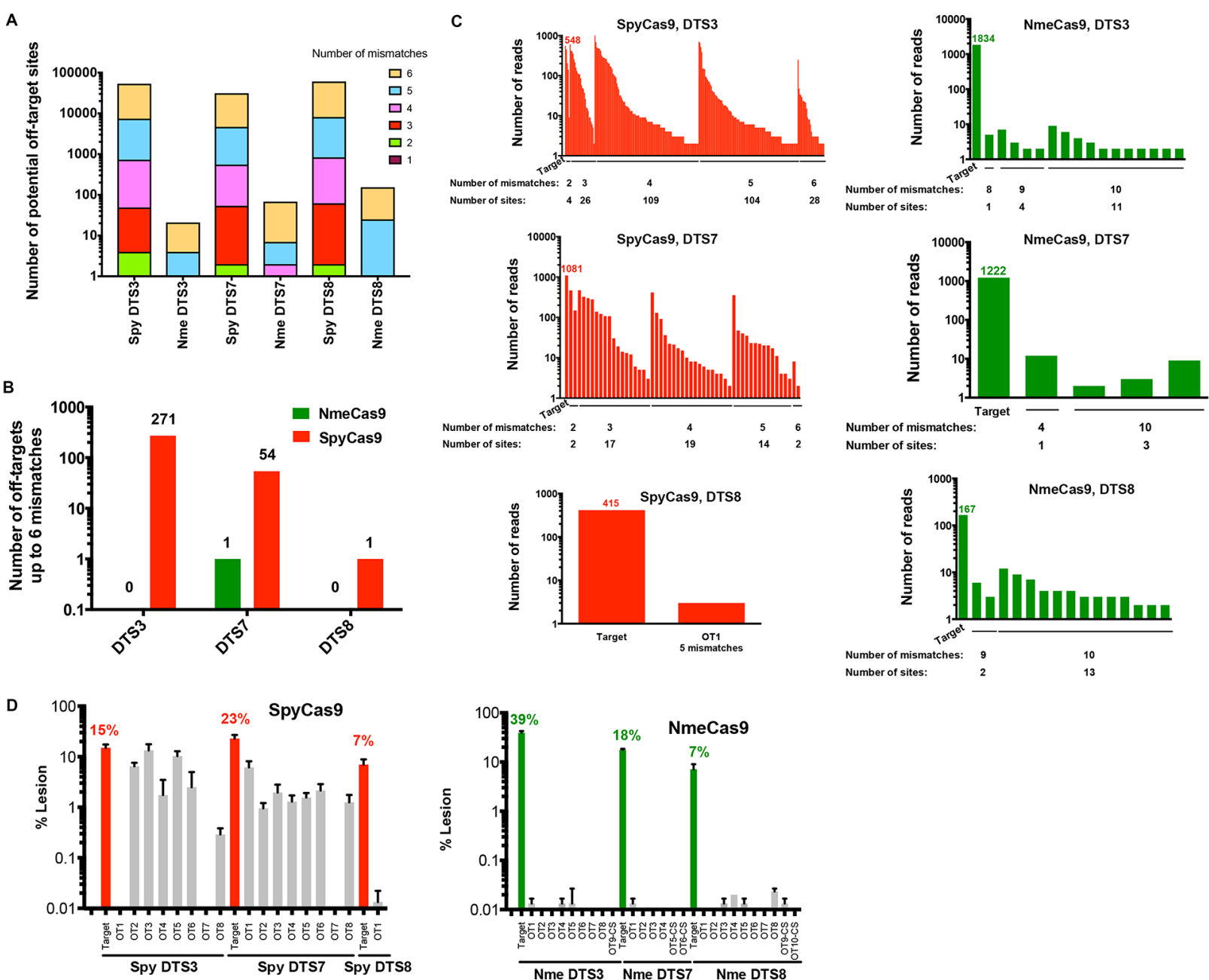
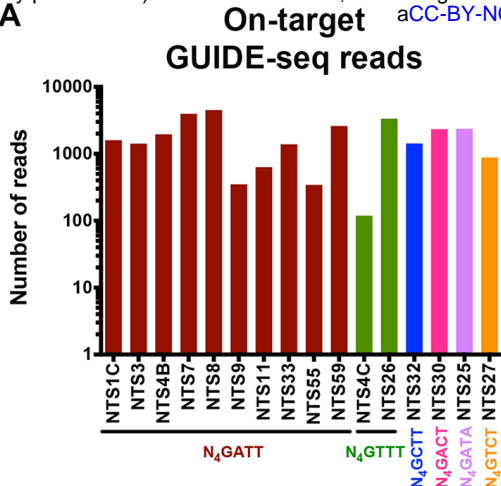
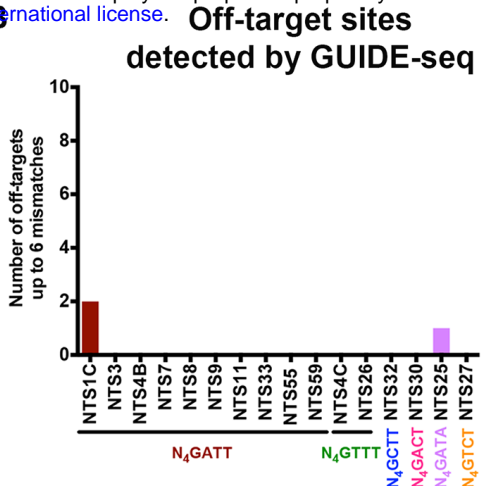


**Figure 6**

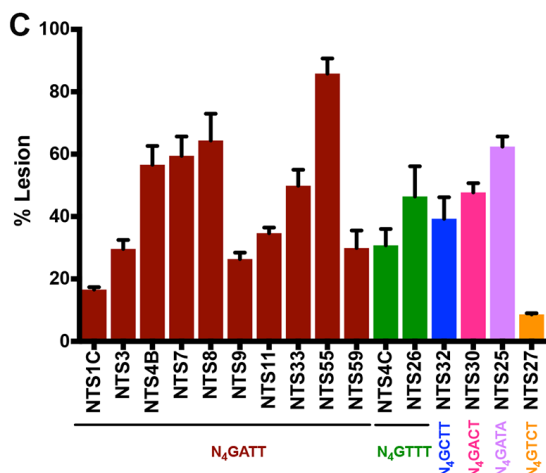
**A**



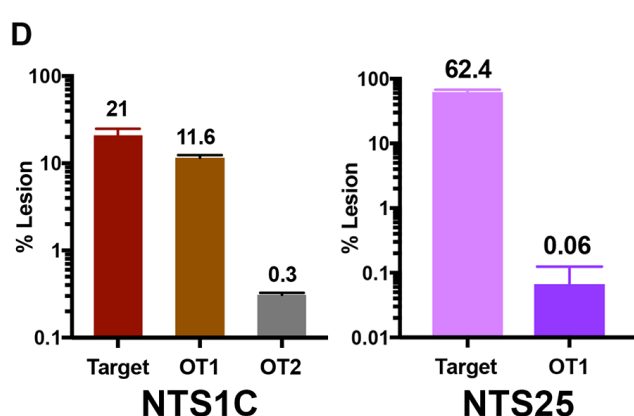
**B**



**C**



**D**



**E**



**F**

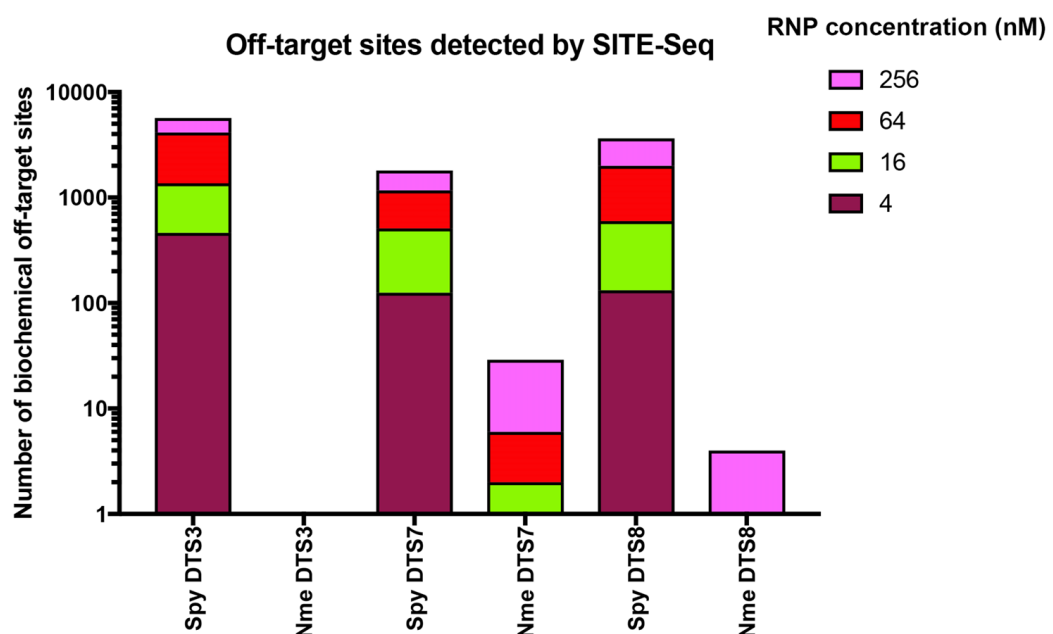


**Figure 7**

bioRxiv preprint doi: <https://doi.org/10.1101/172650>; this version posted May 9, 2018. The copyright holder for this preprint (which was not certified by peer review) is the author/funder, who has granted bioRxiv a license to display the preprint in perpetuity. It is made available under aCC-BY-NC-ND 4.0 International license.

